TPP-SD: Accelerating Transformer Point Process Sampling with Speculative Decoding

Shukai Gong^{1*} Yiyang Fu^{2*} Fengyuan Ran^{3*} Quyu Kong⁴ Feng Zhou^{1†}

¹Center for Applied Statistics and School of Statistics, Renmin University of China

²School of Information, Renmin University of China

³School of Cyber Science and Engineering, Wuhan University

⁴Alibaba Group

^{1,2}{shukai_gong, fuyiyang2022201505, feng.zhou}@ruc.edu.cn

³rfy_Reflow@whu.edu.cn

⁴kongquyu.kqy@alibaba-inc.com

Abstract

We propose TPP-SD, a novel approach that accelerates Transformer temporal point process (TPP) sampling by adapting speculative decoding (SD) techniques from language models. By identifying the structural similarities between thinning algorithms for TPPs and speculative decoding for language models, we develop an efficient sampling framework that leverages a smaller draft model to generate multiple candidate events, which are then verified by the larger target model in parallel. TPP-SD maintains the same output distribution as autoregressive sampling while achieving significant acceleration. Experiments on both synthetic and real datasets demonstrate that our approach produces samples from identical distributions as standard methods, but with $2\text{-}6\times$ speedup. Our ablation studies analyze the impact of hyperparameters such as draft length and draft model size on sampling efficiency. TPP-SD bridges the gap between powerful Transformer TPP models and the practical need for rapid sequence sampling. Code is publicly available at https://github.com/GONGSHUKAI/tppsd.

1 Introduction

Temporal point processes (TPPs) [6] are essential stochastic models for describing discrete event occurrence patterns in continuous time. Classical models include the Poisson process [12], which is history-independent, and the Hawkes process [10, 39, 37], which incorporates historical dependencies. Recently, advancements in deep learning have facilitated the integration of deep models with point processes, significantly enhancing their expressive capabilities in capturing history dependence [19]. Notable examples include models based on traditional RNNs [7], LSTMs [17], and Transformers [40, 36, 20]. RNN-type methods often suffer from vanishing or exploding gradients [26], limiting their performance. In contrast, Transformer TPPs have gained popularity for their ability to capture long-term dependencies and support parallel training.

Most current Transformer TPPs' research focuses on enhancing model expressiveness and training methodologies, with limited attention to improving sampling efficiency. Sampling from a learned temporal point process is essential for synthesizing event sequence data, making predictions based on observed history, validating model goodness-of-fit, and gaining insights into complex process dynamics. The standard sampling procedure employs the thinning algorithm [15, 23], which simulates

^{*}Equal contribution.

[†]Corresponding author.

events from a target process with conditional intensity $\lambda^*(t)$ by iteratively generating candidates \tilde{t}_{i+1} from a simple proposal process (e.g., homogeneous Poisson process with rate $\bar{\lambda}$) and accepting with the probability $\frac{\lambda^*(\tilde{t}_{i+1})}{\bar{\lambda}}$, repeating until acceptance. This is highly inefficient because evaluating the acceptance probability for each proposed candidate requires a forward pass through the Transformer, potentially requiring many forward passes per single accepted event. Despite KV caching [27] reducing inference complexity from quadratic to linear, the large number of parameters in the Transformer architecture makes each forward pass computationally expensive.

Speculative decoding (SD) [5, 14] is a technique designed to accelerate token generation in large language models (LLMs). It generates multiple tokens in parallel, rather than predicting each token sequentially, thereby improving the efficiency of the sampling process. Drawing inspiration from the analogy between next-event sampling in TPPs and next-token prediction in LLMs, we investigate the potential application of SD from LLMs to Transformer TPPs, aiming to enhance sampling efficiency.

Specifically, we make the following key contributions in this work: (1) We identify a strong similarity between the thinning algorithm used in point process sampling and the SD technique in LLMs. (2) We propose TPP-SD, which successfully applies SD to Transformer TPPs, resulting in accelerated sampling. (3) Extensive experiments are conducted on both synthetic and real datasets. The results show that TPP-SD and standard autoregressive sampling produce samples from the same distribution, but TPP-SD achieves a speedup of approximately $2-6\times$. Ablation studies analyze the impact of different hyperparameters.

2 Preliminary Knowledge

In this section, we provide background on TPPs, the thinning algorithm for TPPs, and SD for LLMs.

2.1 Temporal Point Processes

TPPs model discrete event sequences in continuous time, denoted as $S = \{(t_i, k_i)\}_{i=1}^N$ where (t_i, k_i) indicates an event of type $k_i \in \mathcal{K} = \{1, \dots, K\}$ occurring at time $t_i \in (0, T]$, with $0 < t_1 < \dots < t_N \le T$ where N denotes the random number of events. TPPs can be defined using different parameterizations. One approach is to specify the conditional distribution of events. We denote $f(t_{i+1}, k_{i+1} | \mathcal{H}_{t_i})$ to be the conditional density function (CDF) of event (t_{i+1}, k_{i+1}) given the history of previous events $(t_1, k_1), \dots, (t_i, k_i)$. In this work, \mathcal{H}_{t^-} denotes the history of events up to but excluding time t, while \mathcal{H}_t includes whether an event occurs at time t. Consequently, the joint distribution of all events can be factorized as:

$$p(S) = \prod_{i=1}^{N} f(t_i, k_i | \mathcal{H}_{t_{i-1}}) (1 - F(T | \mathcal{H}_{t_N})),$$

where $F(T|\mathcal{H}_{t_N}) = \int_{t_N}^T f(t|\mathcal{H}_{t_N}) \mathrm{d}t$, $f(t|\mathcal{H}_{t_i}) = \sum_{k=1}^K f(t,k|\mathcal{H}_{t_i})$. As is customary, we further decompose $f(t,k|\mathcal{H}_{t_i}) = f(t|\mathcal{H}_{t_i})f(k|\mathcal{H}_{t_i},t)$. The term $(1-F(T|\mathcal{H}_{t_N}))$ is the probability that no event occurs in (t_N,T) . Another approach is to specify the conditional intensity function (CIF):

$$\lambda^*(t,k)dtdk = \frac{f(t,k|\mathcal{H}_{t_i})dtdk}{1 - F(t|\mathcal{H}_{t_i})} = \mathbb{E}[N(dt \times dk)|\mathcal{H}_{t^-}],$$

where * indicates that the CIF is dependent on the history \mathcal{H}_{t^-} . These different parameterizations are equivalent because it can be easily proven that the CIF $\lambda^*(t,k)$ and the CDF $f(t,k|\mathcal{H}_{t_i})$ are one-to-one [38]. It is worth noting that the event timestamps can also be equivalently expressed as inter-event intervals $\tau_i = t_i - t_{i-1}, \ i = 1, \dots, N$ with $t_0 = 0$. Therefore, the CDF of the timestamps can also be equivalently expressed as the CDF of the inter-event intervals $g(\tau|\mathcal{H}_{t_i}) = f(t_i + \tau|\mathcal{H}_{t_i})$. Correspondingly, TPPs have two equivalent forms of log-likelihood expression:

$$\log p(\mathcal{S}) = \sum_{i=1}^{N} \log \lambda^*(t_i, k_i) - \sum_{k=1}^{K} \int_0^T \lambda^*(t, k) dt$$
 (1)

$$= \sum_{i=1}^{N} \left[\log g(\tau_i | \mathcal{H}_{t_{i-1}}) + \log f(k_i | \mathcal{H}_{t_{i-1}}, t_i) \right] + \log(1 - G(T | \mathcal{H}_{t_N})), \tag{2}$$

where $G(T|\mathcal{H}_{t_N})=\int_0^{T-t_N}g(\tau|\mathcal{H}_{t_N})\,\mathrm{d}\tau$. Eq. (1) is CIF-based, and Eq. (2) is CDF-based.

2.2 Thinning Algorithm for TPPs

For illustration purposes, we discuss the sequential simulation of timestamps from a point process using the thinning algorithm. Given the event history \mathcal{H}_{t_i} , to sample a timestamp from the original point process model (denoted as OriP) parameterized by CIF $\lambda^*(t)$, we use a proposal point process, typically a homogeneous Poisson process (denoted as PoiP) with intensity $\bar{\lambda} = \sup_{t \in (t_i, \infty)} \lambda^*(t)$, to sample the next candidate timestamp:

$$\tilde{t}_{i+1} \sim \text{PoiP}(\mathcal{H}_{t_i}).$$

Next, the original point process model evaluates the candidate timestamp by calculating the conditional intensity at the given position:

$$\lambda^*(\tilde{t}_{i+1}) = \text{OriP}(\tilde{t}_{i+1}; \mathcal{H}_{t_i}).$$

Then, a rejection sampling step is applied to verify the candidate timestamp. The \tilde{t}_{i+1} is accepted if

$$\epsilon < \frac{\lambda^*(\tilde{t}_{i+1})}{\bar{\lambda}}, \quad \epsilon \sim \mathrm{Uniform}[0,1].$$

This rejection sampling ensures that the final sequence adheres to the original point process distribution. If the candidate timestamp is rejected, the process is repeated until a candidate is accepted. The accepted timestamp is then added to the event history, forming $\mathcal{H}_{t_{i+1}}$, and the procedure continues until the sequence is fully generated. The efficiency of the thinning algorithm depends heavily on the alignment between the proposal point process and the original point process. A closer alignment results in a higher acceptance rate, improving overall performance.

2.3 Speculative Decoding for LLMs

Autoregressive sampling in LLMs is inherently sequential and inefficient. SD addresses this inefficiency by delegating auto-regressive sampling to a smaller language model (draft model, denoted as LLM_{dra}), which generates multiple candidate tokens sequentially given the context s:

$$(c_1, q_1), \ldots, (c_{\gamma}, q_{\gamma}) \sim \text{LLM}_{dra}(\mathbf{s}),$$

where γ is the length of candidate tokens, c_1, \ldots, c_{γ} are the sampled tokens, and q_1, \ldots, q_{γ} are their corresponding probability distributions. Then, the original language model (target model, denoted as LLM_{tar}) processes these candidate tokens in parallel, producing probability distributions:

$$p_1, \ldots, p_{\gamma+1} = \text{LLM}_{\text{tar}}(c_1, \ldots, c_{\gamma}; \mathbf{s}),$$

where the extra probability distribution $p_{\gamma+1}$ corresponds to processing the candidate token c_{γ} . A sequence of token-level rejection sampling is then applied to verify the candidate tokens. A candidate token c_i is accepted if all previous tokens are accepted and

$$\epsilon_i < \frac{p_i(c_i)}{q_i(c_i)}, \quad \epsilon_i \sim \text{Uniform}[0, 1].$$

This rejection sampling ensures that the final sequence adheres to the distribution of the target model. If c_i is the first rejected token, a replacement can be sampled from an adjusted distribution $\operatorname{norm}(\max(0,p_i-q_i))$. When all candidates are accepted, an additional token is sampled from $p_{\gamma+1}$. The accepted tokens are then added to the context s, and the process repeats until the sequence is complete. The efficiency of SD heavily depends on the alignment between the draft and target models. A closer alignment leads to a higher acceptance rate, improving overall performance.

3 Related Works

In this section, we discuss related works on point process sampling. In traditional statistical point processes, the CIF parameterization is generally preferred because the CDF is not a convenient way to specify history-dependent point processes. In contrast, the CIF provides a more convenient way to specify how the present depends on the past. Therefore, sampling methods in the statistical point process field are generally based on the CIF. Inverse method [28] simulates a unit-intensity

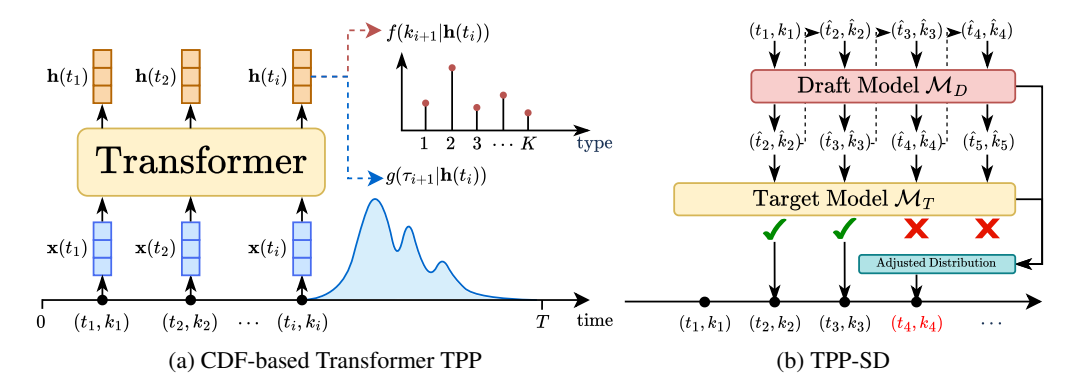


Figure 1: (a) Overall architecture of our proposed CDF-based Transformer TPP. (b) The visualization of our proposed TPP-SD sampling method as elaborated in Section 4.3.

Poisson process and transforms it into the desired point process using the inverse of the integrated CIF, leveraging the time-rescaling theorem [2], and [30] applies the inverse map in parallel to accelerate this process. However, this method is not suitable for complex processes that do not have analytical forms for the inverse of integrated CIF. Another more easily implementable sampling method is the thinning algorithm, which was originally proposed for sampling from inhomogeneous Poisson processes [15], and later adapted for history-dependent processes [23, 31]. With the development of the deep neural point process, an increasing number of works have started using the CDF parameterization. For example, [29] used normalizing flows and mixtures of log-normal densities to model the CDF of the inter-event interval. Although this approach was initially proposed for training convenience, another advantage it brings is facilitating sampling. This is because we can easily sample the next event directly from the CDF [24]. Whether based on CIF or CDF, both of the above methods for sampling history-dependent point processes can only be performed sequentially, leading to inefficient sampling. The key difference of this work is the introduction of parallelization in sampling, which accelerates the sampling process.

4 Methodology

In this section, we analyze the similarity between the thinning algorithm and the SD technique. Inspired by this insight, we propose one SD method for Transformer TPP models.

4.1 Thinning Algorithm v.s. Speculative Decoding

As introduced in Sections 2.2 and 2.3, the thinning algorithm and SD share significant structural similarities despite their different application domains. Both methods adopt a two-stage "proposeverify" framework that uses a draft model to generate candidates and uses the target model for verification. Besides, the efficiency of both methods critically depends on the alignment between the proposal and target distributions.

Despite these similarities, several key differences distinguish these approaches. The thinning algorithm operates strictly in an autoregressive manner, generating and verifying a single candidate timestamp per propose-verify iteration. In contrast, SD can propose and validate multiple tokens per propose-verify iteration, resulting in accelerated sampling. Additionally, while the thinning algorithm may fail to produce a valid timestamp per propose-verify iteration, SD guarantees the generation of at least one valid token per propose-verify iteration.

Motivated by these observations—especially the algorithmic similarities and the limitations of the thinning algorithm—we propose TPP-SD: a novel CDF-based sampling method for Transformer TPPs that applies the principles of SD to enhance sampling efficiency.

4.2 CDF-based Transformer TPPs

To accelerate TPP sampling using SD, we first need to design a CDF-based Transformer TPP model, which is composed of two parts. A similar model design has also been adopted by [24].

Encoder. We use Transformer backbones to model the historical dependencies in the event sequence. Specifically, given an observed realization of the point process $\mathcal{S} = \{(t_i, k_i)\}_{i=1}^N$, we apply the temporal encoding method from [40] to encode each timestamp t_i into a fixed-length vector $\mathbf{z}(t_i) \in \mathbb{R}^D$. In addition to the temporal encoding, we use an embedding matrix $\mathbf{W} \in \mathbb{R}^{K \times D}$, where the D-dimensional embedding for event type k_i is given by $\mathbf{W}^{\top}\mathbf{k}_i$, with $\mathbf{k}_i \in \mathbb{R}^K$ being the one-hot encoding of k_i . Thus, the embedding for the observed realization is given by

$$\mathbf{X} = f(\mathbf{KW}, \mathbf{Z}) \in \mathbb{R}^{N \times D}$$

where $\mathbf{K} = [\mathbf{k}_1, \dots, \mathbf{k}_N]^{\top} \in \mathbb{R}^{N \times K}$ and $\mathbf{Z} = [\mathbf{z}_1, \dots, \mathbf{z}_N]^{\top} \in \mathbb{R}^{N \times D}$ are the collections of event types and timestamp embeddings of the observed realization, and $f(\cdot, \cdot)$ is a fusion function where we use a summation operation. A Transformer is then applied to obtain the history embedding matrix $\mathbf{H} = T_{\theta}(\mathbf{X}) \in \mathbb{R}^{N \times D}$. Each row of the history embedding matrix $\mathbf{h}^{\top}(t_i) = \mathbf{H}(i, :) \in \mathbb{R}^D$ corresponds to the history information up to timestamp t_i . The choice of encoder T_{θ} can be any Transformer TPP, such as THP [40], SAHP [36], or AttNHP [18]. The necessity of using a Transformer encoder lies in its ability to enable parallel computation, which is essential for SD.

Decoder. Inspired by [24, 29], to enhance the flexibility of the model, we use a mixture of log-normal distributions to model the CDF of the next timestamp $g(\tau_{i+1}|\mathbf{h}(t_i))$, since the inter-event intervals are positive, i.e.,

$$g_{\theta}(\tau_{i+1}|\mathbf{h}(t_i)) = \sum_{m=1}^{M} w_{im} \frac{1}{\tau \sqrt{2\pi}\sigma_{im}} \exp\left(-\frac{(\log \tau_{i+1} - \mu_{im})^2}{2\sigma_{im}^2}\right).$$

Here, $g_{\theta}(\tau_{i+1}|\mathbf{h}(t_i))$ is referred to as the decoder because it takes the history embedding $\mathbf{h}(t_i)$ as input and decodes the inter-event intervals. The mixture weights $\mathbf{w}_i = [w_{i1}, \dots, w_{iM}]^{\top}$, the mixture means $\boldsymbol{\mu}_i = [\mu_{i1}, \dots, \mu_{iM}]^{\top}$, and the mixture standard deviations $\boldsymbol{\sigma}_i = [\sigma_{i1}, \dots, \sigma_{iM}]^{\top}$ are obtained by mapping $\mathbf{h}(t_i)$. Specifically, $\mathbf{h}(t_i) \in \mathbb{R}^D$ is projected to $\mathbf{e}_i = \mathbf{E}\mathbf{h}(t_i) \in \mathbb{R}^{3D}$ with $\mathbf{E} \in \mathbb{R}^{3D \times D}$, and then sliced into three equal-length parts $\mathbf{e}_i = \begin{bmatrix} \mathbf{e}_i^{i\top}, \mathbf{e}_2^{i\top}, \mathbf{e}_3^{i\top} \end{bmatrix}^{\top}$. Subsequently, $\mathbf{e}_i^i, \mathbf{e}_2^i, \mathbf{e}_3^i$ are mapped to $\mathbf{w}_i, \boldsymbol{\mu}_i$, and $\boldsymbol{\sigma}_i$ as follows:

$$\mathbf{w}_i = \operatorname{softmax}(\mathbf{V}_{\mathbf{w}}\mathbf{e}_1^i + \mathbf{b}_{\mathbf{w}}), \quad \boldsymbol{\mu}_i = \mathbf{V}_{\boldsymbol{\mu}}\mathbf{e}_2^i + \mathbf{b}_{\boldsymbol{\mu}}, \quad \boldsymbol{\sigma}_i = \exp(\mathbf{V}_{\boldsymbol{\sigma}}\mathbf{e}_3^i + \mathbf{b}_{\boldsymbol{\sigma}}),$$

where $\mathbf{V_w}, \mathbf{V_{\mu}}, \mathbf{V_{\sigma}} \in \mathbb{R}^{M \times D}$, and $\mathbf{b_w}, \mathbf{b_{\mu}}, \mathbf{b_{\sigma}} \in \mathbb{R}^M$ are learnable parameters. The CDF of the next event type $f_{\theta}(k_{i+1}|\mathbf{h}(t_i))$ is modeled as a categorical distribution:

$$f_{\boldsymbol{\theta}}(k_{i+1}|\mathbf{h}(t_i)) = \operatorname{softmax}\left(\mathbf{V}_{\mathbf{k}}^{(2)} \tanh(\mathbf{V}_{\mathbf{k}}^{(1)}\mathbf{h}(t_i) + \mathbf{b}_{\mathbf{k}}^{(1)}) + \mathbf{b}_{\mathbf{k}}^{(2)}\right).$$

Our proposed CDF-based Transformer TPP model is illustrated in Fig. 1a. This model can be formally represented as $\mathcal{M}=\{\mathcal{E},g(\tau|\cdot),f(k|\cdot)\}$, where \mathcal{E} corresponds to the encoder and $g(\tau|\cdot),f(k|\cdot)$ correspond to the decoder. The model is trained by maximizing the log-likelihood in Eq. (2).

Naïve autoregressive sampling. The next timestamp is easy to sample from the log-normal mixture distribution $g_{\theta}(\tau_{i+1}|\mathbf{h}(t_i))$ by (see Appendix A.1 for proof)

$$\mathbf{z}_i \sim \text{Categorical}(\mathbf{w}_i), \quad \epsilon \sim \mathcal{N}(0, 1), \quad \hat{\tau}_{i+1} = \exp(\boldsymbol{\mu}_i^{\top} \mathbf{z}_i + \epsilon \cdot \boldsymbol{\sigma}_i^{\top} \mathbf{z}_i),$$

so the next timestamp is $\hat{t}_{i+1} = t_i + \hat{\tau}_{i+1}$. The next event type is sampled by $\hat{k}_{i+1} \sim f_{\theta}(k_{i+1}|\mathbf{h}(t_i))$. The new event $(\hat{t}_{i+1}, \hat{k}_{i+1})$ is appended to the history and the sampling procedure is repeated until we reach the predetermined end time. However, naïve autoregressive sampling requires a forward pass of the Transformer encoder for each event, which becomes inefficient as the number of parameters in the Transformer backbone increases.

4.3 TPP-SD

Suppose we have a trained target Transformer TPP model \mathcal{M}_T with a large number of parameters, from which we wish to sample events, and a trained draft Transformer TPP model \mathcal{M}_D with fewer parameters, which we use to approximate \mathcal{M}_T . The procedure of TPP-SD consists of three steps, as shown in Fig. 1b and Algorithm 1.

Drafting. Sample γ candidate events $\{(\hat{t}_{i+1}, \hat{k}_{i+1}), \dots, (\hat{t}_{i+\gamma}, \hat{k}_{i+\gamma})\}$ autoregressively from \mathcal{M}_D . Meanwhile, we record the interval CDF $g_D(\hat{\tau}_{i+l}|\cdot)$ and type CDF $f_D(\hat{k}_{i+l}|\cdot)$ for all candidate events.

Verification. Run \mathcal{M}_T in parallel to compute $g_T(\hat{\tau}_{i+l}|\cdot)$ and $f_T(\hat{k}_{i+l}|\cdot)$ for all candidate events. Then, calculate the acceptance rates $\frac{g_T(\hat{\tau}_{i+l}|\cdot)}{g_D(\hat{\tau}_{i+l}|\cdot)}$ and $\frac{f_T(\hat{k}_{i+l}|\cdot)}{f_D(\hat{k}_{i+l}|\cdot)}$ for all candidate events. A candidate inter-event interval $\hat{\tau}_{i+l}$ is accepted if all previous events are accepted and $\epsilon_l^{\tau} < \frac{g_T(\hat{\tau}_{i+l}|\cdot)}{g_D(\hat{\tau}_{i+l}|\cdot)}, \epsilon_l^{\tau} \sim$ Uniform[0, 1]. A candidate event type \hat{k}_{i+l} is accepted if all previous events and $\hat{\tau}_{i+l}$ are accepted, and $\epsilon_l^{k} < \frac{f_T(\hat{k}_{i+l}|\cdot)}{f_D(\hat{k}_{i+l}|\cdot)}, \epsilon_l^{k} \sim$ Uniform[0, 1].

Sampling from adjusted distribution. Once a candidate event interval $\hat{\tau}_{i+l}$ or type \hat{k}_{i+l} is rejected, all subsequent candidate events are automatically discarded and a replacement $\hat{\tau}_{i+l}$ or \hat{k}_{i+l} is sampled from an adjusted distribution defined as below:

$$g'(\tau_{i+l}|\cdot) = \operatorname{norm}(\max(0, g_T(\tau_{i+l}|\cdot) - g_D(\tau_{i+l}|\cdot))), \tag{3}$$

$$f'(k_{i+l}|\cdot) = \text{norm}(\max(0, f_T(k_{i+l}|\cdot) - f_D(k_{i+l}|\cdot))), \tag{4}$$

where $norm(\cdot)$ denotes the normalization. The correctness and necessity of sampling from the adjusted distribution have been established in the original speculative decoding work for LLMs [14]. In this work, we extend the proof to the TPP domain, as presented in Appendix A.2.

Eq. (4) is a discrete distribution, and its normalization is relatively easy to implement, but Eq. (3) is a continuous distribution, and normalizing it is much more difficult because we need to compute the normalizing constant $\int \max(0, g_T(\tau_{i+l}|\cdot) - g_D(\tau_{i+l}|\cdot))d\tau_{i+l}$. This is also the main difference between TPP-SD and LLM-SD, as continuous distributions are not involved in the LLM application. Inspired by [32], we employ an acceptance-rejection sampling scheme [4] to sample from $g'(\tau_{i+l}|\cdot)$, as outlined in Theorem 1 (refer to Appendix A.3 for the proof).

Theorem 1. For a sample $\hat{\tau}_{i+l} \sim g_T(\tau_{i+l}|\cdot)$, define the acceptance threshold as

$$\alpha = \frac{\max\left(0, g_T(\hat{\tau}_{i+l}|\cdot) - g_D(\hat{\tau}_{i+l}|\cdot)\right)}{g_T(\hat{\tau}_{i+l}|\cdot)}.$$

Accept $\hat{\tau}_{i+l}$ if $\epsilon < \alpha$, where $\epsilon \sim Uniform(0,1)$. This acceptance-rejection procedure generates samples from the adjusted distribution $g'(\tau_{i+l}|\cdot)$ defined in Eq. (3).

5 Experiments

In this section, we compare TPP-SD with autoregressive sampling (abbreviated as AR sampling) on both synthetic and real datasets. We verify that both methods produce samples from the same underlying distribution, and demonstrate that TPP-SD significantly improves sampling efficiency.

5.1 Evaluation of Sampling Quality and Speed

Unlike point process fitting, which focuses on the accuracy of predicted event types or timestamp deviations, point process sampling emphasizes whether the samples generated by TPP-SD and AR sampling follow the same distribution (i.e., sampling quality), as well as the efficiency of the sampling process (i.e., sampling speed). Therefore, we define the following evaluation metrics.

Likelihood Discrepancy (Synthetic and Real). For synthetic data, where the ground truth is known, we generate samples using both AR sampling and TPP-SD, and measure the discrepancy between the ground-truth likelihood (Eq. (1)) and the model likelihood of the generated samples (Eq. (2)). Specifically, we compute $\Delta \mathcal{L}_{ar}^{syn} = |\mathcal{L}_{gt} - \mathcal{L}_{ar}|$ for AR sampling and $\Delta \mathcal{L}_{sd}^{syn} = |\mathcal{L}_{gt} - \mathcal{L}_{sd}|$ for TPP-SD. For real data, where the ground truth is unknown, we measure the discrepancy between the AR sampling likelihood and the TPP-SD likelihood, $\Delta \mathcal{L}^{real} = |\mathcal{L}_{ar} - \mathcal{L}_{sd}|$. Ideally, samples generated by TPP-SD and AR sampling should follow the same distribution—i.e., the ground-truth distribution. A lower likelihood discrepancy indicates higher sample quality.

Table 1: Performance of TPP-SD with draft length $\gamma=10$ against AR sampling across synthetic datasets and Transformer encoders. We conduct all experiments using three random seeds and report the mean for each metric. For all metrics, the best performance is highlighted in **bold**.

D	ataset	1	Poissor	1		Hawke	8	Multi-Hawkes		kes
Enco	der Type	THP	SAHP	AttNHP	THP	SAHP	AttNHP	THP	SAHP	AttNHP
$\Delta \mathcal{L}^{\text{syn}}\left(\downarrow\right)$	AR Sampling TPP-SD	0.542 0.349	0.012 0.204	1.879 1.952	0.753 0.276	0.884 0.630	0.220 0.722	0.022 0.321	0.146 0.070	0.334 0.199
$D_{\mathrm{KS}}\left(\downarrow\right)$	AR Sampling TPP-SD	0.038 0.036	0.033 0.050	0.076 0.068	0.044	0.031 0.028	0.029 0.027	0.069 0.053	0.055 0.080	0.065 0.045
Wall-time $T(\downarrow)$	AR Sampling TPP-SD	3.477 1.647	2.680 2.077	12.103 4.063	5.147 2.547	2.747 1.863	20.503 3.567	4.007 1.893	2.490 1.647	12.403 2.770
Speedup Ratio $S_{AR/SD}$ (\uparrow)		2.110	1.290	2.967	2.113	1.513	5.743	2.117	1.277	4.467

Kolmogorov-Smirnov Statistic (Synthetic Only). For synthetic data where the ground truth is known, the time-rescaling theorem [2] states that for event times $\{t_i\}_{i=1}^n$ generated by a point process with CIF $\lambda^*(t)$, if the model is correctly specified, the transformed inter-event intervals $z_i = \int_{t_{i-1}}^{t_i} \lambda^*(\tau) d\tau$ are i.i.d. samples from Exponential(1). Therefore, we apply the ground-truth CIF to transform the samples generated by AR sampling and TPP-SD, and then compute the KS statistic $D_{\rm KS}$ to assess the conformity of generated samples to the ground-truth distribution. A smaller $D_{\rm KS}$ indicates higher sample quality. The detailed computation of $D_{\rm KS}$ is provided in Appendix A.4.

Wasserstein Distance (Real Only). For real data where the ground truth is unknown, the KS statistic cannot be computed. Instead, we assess the sampling consistency between AR sampling and TPP-SD using the Wasserstein distance $D_{\rm WS}$. Specifically, using the first M events as history, we perform N independent repetitions of sampling (M+1)-th event, yielding $\{(t_i^{\rm AR},k_i^{\rm AR})\}_{i=1}^N$ from AR sampling and $\{(t_i^{\rm SD},k_i^{\rm SD})\}_{i=1}^N$ from TPP-SD. For the temporal distribution, we compute $D_{\rm WS}^t$, the 1-Wasserstein distance between the empirical distributions of $\{t_i^{\rm AR}\}_{i=1}^N$ and $\{t_i^{\rm SD}\}_{i=1}^N$, using ot .wasserstein_1d from the POT library [9]. For the event type distribution, we compute $D_{\rm WS}^k$, the earth mover's distance between the empirical distributions of $\{k_i^{\rm AR}\}_{i=1}^N$ and $\{k_i^{\rm SD}\}_{i=1}^N$, using ot .emd2 from the same library. A smaller $D_{\rm WS}$ indicates higher sample quality.

Speedup Ratio (Synthetic and Real). Sampling efficiency is central to this work. We quantify the acceleration gain by computing the ratio of execution wall times between AR sampling and TPP-SD, defined as $S_{\text{AR/SD}} = \frac{T_{\text{AR}}}{T_{\text{SD}}}$, where T_{AR} and T_{SD} denote the execution wall times of AR sampling and TPP-SD, respectively. A larger $S_{\text{AR/SD}}$ indicates a faster sampling speed.

5.2 Experimental Results on Synthetic Data

Datasets and Setup. We consider three synthetic datasets: inhomogeneous Poisson, univariate Hawkes, and multivariate Hawkes processes, each with 1000 sequences within the time window [0, 100]. For each dataset, we train an 8-head, 20-layer target model and a 1-head, 1-layer draft model. We compare two sampling approaches: AR sampling using only the target model versus TPP-SD which combines both target and draft models as elaborated in Section 4.3. Details on data simulation procedures, data splitting, and experimental settings are provided in Appendices B.1 and C.3.1.

Results. As shown in Table 1, across all three synthetic datasets and three encoder architectures, TPP-SD consistently demonstrates high-fidelity sampling that closely matches the performance of AR sampling. Specifically, both TPP-SD and AR sampling exhibit low likelihood discrepancies and near-zero KS statistics relative to the ground truth, indicating excellent alignment with the target distribution. Furthermore, as shown in Fig. 2, the KS plots show that the samples generated by both methods consistently fall within the 95% confidence bands.

TPP-SD consistently achieves faster execution times and $1.3-5.7 \times$ speedup across all datasets and encoder architectures. These results demonstrate that TPP-SD maintains the same high sampling fidelity as AR sampling while providing significant improvements in sampling efficiency.

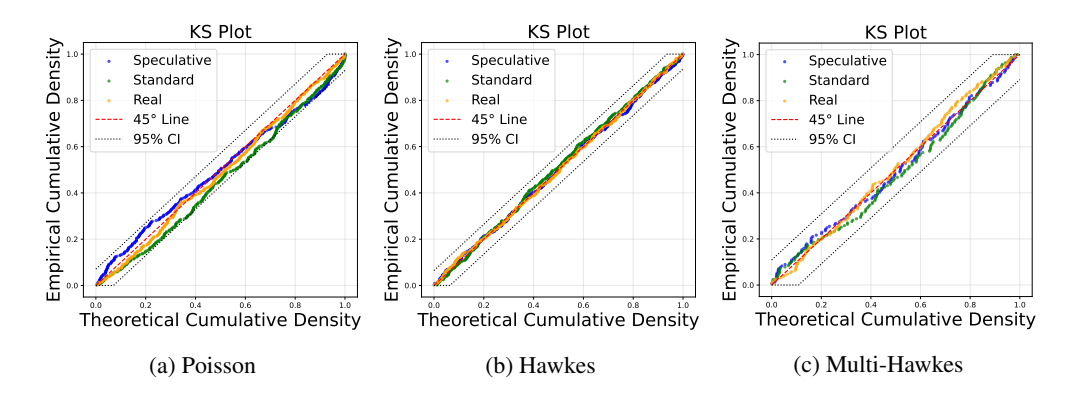


Figure 2: KS plots for (a) Poisson, (b) Hawkes, and (c) Multi-Hawkes datasets. We use AttNHP as encoder, and blue, green, and orange points represent samples from TPP-SD ($\gamma=10$), AR sampling, and ground truth, respectively. Black dotted lines show 95% KS confidence bands.

Table 2: Performance of TPP-SD with draft length $\gamma=10$ against AR sampling across real datasets and Transformer encoders. We conduct all experiments using three random seeds and report the mean for each metric. For all metrics, the best performance is highlighted in **bold**.

Dataset		Taobao)	Amazon			Taxi			StackOverflow		
Enco	der Type	THP	SAHP	AttNHP THP	SAHP	AttNHP	THP	SAHP	AttNHP	THP	SAHP	AttNHP	
$\Delta \mathcal{L}^{\text{real}}\left(\downarrow\right)$	AR Sampling TPP-SD	0.446 0.033	0.148 0.746	0.629 0.056 0.860 0.129	0.099 0.035		1.4411 0.065	0.563 0.093	0.859 0.506	0.587 0.231	0.340 0.602	0.985 0.020	
$D_{\mathrm{WS}}^{t}\left(\downarrow\right)$	AR Sampling TPP-SD	0.236 0.076	0.328 0.493	0.187 0.189 0.116 0.078	0.019 0.146		0.201 0.082	0.236 0.036	0.249 0.331	0.470 0.391	0.378 0.518	0.677 0.614	
$D_{\mathrm{WS}}^{k}\left(\downarrow\right)$	AR Sampling TPP-SD	0.267 0.751	0.414 0.368	0.193 0.184	0.459 1.409		0.055 0.655	0.778 0.744	0.094 0.134	0.376 0.375	0.381 0.199	0.218 0.507	
Wall-time $T(\downarrow)$	AR Sampling TPP-SD	5.890 3.460	2.460 1.643	16.256 1.023 5.180 0.290	0.900 0.317		1.157 0.453	1.183 0.347	2.573 0.650	1.353 0.700	1.423 0.663	3.217 0.783	
Speedup R	atio $S_{AR/SD}$ (†)	1.597	1.553	3.183 3.550	2.847	5.849	2.553	3.637	4.310	1.930	2.153	4.290	

In addition, architectural variations are evident: AttNHP achieves the highest acceleration ratios despite having the slowest wall times; SAHP shows the lowest speedup but maintains the fastest wall times; and THP strikes a balance between acceleration ratio and runtime. These results suggest that the underlying architecture plays a significant role in determining the effectiveness of acceleration. A detailed discussion of these differences is provided in Appendix D.4.

5.3 Experimental Results on Real Data

Datasets and Setup. For real data, we consider four commonly used datasets: **Taobao** [1], **Amazon** [22], **Taxi** [33], and **StackOverflow** [8]. We similarly train an 8-head, 20-layer target model and a 1-head, 1-layer draft model as in Section 5.2, and compare the sampling performance between AR sampling and TPP-SD. Details on data statistics, data splitting, and experimental settings are provided in Appendix C.3.2. It is worth noting that for real data, the ground-truth distribution is unknown. Therefore, we use AR sampling as a reference and quantify how closely TPP-SD approximates it. To establish a meaningful baseline that accounts for the inherent stochasticity of TPP sampling, we compare two independent runs of AR sampling. In theory, the likelihood discrepancy and Wasserstein distances between two such runs should be zero. However, due to stochastic variation, even independent autoregressive runs may exhibit small differences. This self-comparison serves as a baseline for evaluating how well TPP-SD aligns with AR sampling.

Results. Table 2 shows TPP-SD consistently delivers high-fidelity sampling across all real datasets and encoder architectures. Similar to the observations on synthetic data, $\Delta \mathcal{L}^{\text{real}}$ remains low, and both D_{WS}^t approach zero, indicating strong alignment in both temporal and type distributions. Moreover, TPP-SD achieves $1.6-5.9 \times$ faster execution across all settings. These results confirm that TPP-SD matches the sampling fidelity of AR sampling while offering substantial gains in efficiency.

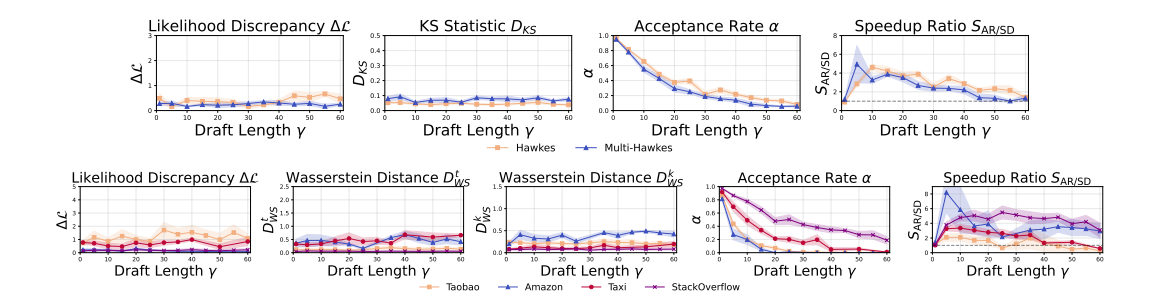


Figure 3: The impact of draft length γ on sampling quality measured by likelihood discrepancy ($\Delta \mathcal{L}$) and distance ($D_{\rm KS}$ or $D_{\rm WS}$), and on sampling speed measured by speedup ratio $S_{\rm AR/SD}$. We conduct all experiments using five random seeds and report the mean and the error band for each metric.

Table 3: Performance of TPP-SD with draft length $\gamma=10$ under different size of draft model. The distance metrics $D_{\rm KS}$ is used for synthetic datasets, while $D_{\rm WS}^t$ and $D_{\rm WS}^k$ are used for real datasets. We conduct all experiments using three random seeds and report the mean for each metric. For all metrics, the best performance is highlighted in **bold**, and the second best is highlighted in <u>underline</u>.

Dataset	Encoder	Draft Model		$\Delta \mathcal{L}$	Distance			α (†)	Wall-time		Speedup Ratio
Dataset	Type	head	layer	<u>\(\(\) \(\) \(\) \(\)</u>	$ \begin{array}{c ccccccccccccccccccccccccccccccccccc$	$S_{AR/SD} (\uparrow)$					
		1	1	0.098	0.011	-	-	0.600	12.403	2.650	4.680
Multi-Hawkes	AttNHP	2	4	0.139	0.009	-	-	0.710	12.403	3.003	4.130
		4	6	0.227	0.004	-	-	0.740	12.403	5.176	2.676
		1	1	0.276	-	0.080	0.197	0.220	16.256	5.727	2.838
Taobao	AttNHP	2	4	0.174	-	0.129	0.200	0.300	16.256	6.513	2.496
		4	6	0.371	-	0.131	0.190	0.35	16.256	8.81	1.845

An interesting observation is that the speedup inversely correlates with event type cardinality. Datasets with higher cardinality (K=17 for Taobao, K=22 for StackOverflow) tend to yield lower speedup compared to those with lower cardinality (K=16 for Amazon, K=10 for Taxi). This is because a larger number of event types increases the probability of divergence between the draft and target models, leading to more rejections during SD. Additionally, the AttNHP encoder consistently achieves greater speedups than THP and SAHP, a trend also observed in the synthetic data experiments.

5.4 Ablation Studies

We analyze the sensitivity of two critical hyperparameters, draft length γ and draft model size. Throughout this part, we adopt AttNHP encoder, and record the likelihood discrepancy $\Delta\mathcal{L}$ ($\Delta\mathcal{L}_{\rm sd}^{\rm syn}$ for synthetic and $\Delta\mathcal{L}^{\rm real}$ for real datasets), distance metrics D ($D_{\rm KS}$ for synthetic and $D_{\rm WS}$ for real datasets), acceptance rate $\alpha = \frac{\text{\# events accepted}}{\text{\# events drafted}}$, wall time T and speedup ratio $S_{\rm AR/SD}$.

Draft Length. To identify the optimal draft length γ for TPP-SD, we evaluate performance across datasets within the time window [0,100] for $\gamma \in [1,60]$. Fig. 3 shows that variations in γ have negligible impacts on the metrics $\Delta \mathcal{L}$ and D, confirming the distributional equivalence of TPP-SD and AR sampling. However, acceptance rate α decreases as γ increases, and speedup $S_{\text{AR/SD}}$ peaks before declining—falling below $1\times$ for excessively large draft lengths due to the overhead of evaluating rejected drafts. Moderate draft lengths (e.g., $\gamma \approx 5$ –15) yield the highest speedup across all datasets.

Draft Model Size. We investigate the impact of draft model size on performance by fixing the target model to an 8-head, 20-layer Transformer and evaluating three draft configurations: 1-head-1-layer, 2-head-4-layer, and 4-head-6-layer. Experiments are conducted on the Multi-Hawkes and Taobao datasets. Results show that increasing draft model size preserves sampling quality—as measured by $\Delta \mathcal{L}$ and D—and improves the acceptance rate α , but reduces the speedup ratio $S_{\text{AR/SD}}$. Notably, the 1-head-1-layer configuration achieves the highest speedup without compromising sample quality.

6 Conclusions

In this work, we introduce the original SD framework from the LLM domain into the context of TPP sampling. By identifying structural similarities between the thinning algorithm in TPPs and speculative decoding in LLMs, we develop an efficient framework that employs a lightweight draft model to propose candidate events for verification by the target model. TPP-SD significantly improves sampling efficiency by $2-6\times$ while preserving distributional consistency with AR sampling, thus bridging the gap between the expressive power of Transformer TPPs and the need for efficient sequence generation in practical applications. As future work, we plan to further optimize TPP-SD by incorporating advancements in SD. Specifically, we aim to integrate the draft mechanism into the target model [3], or perform speculative decoding at the feature level rather than the event level [16].

Acknowledgments

This work was supported by the NSFC Project (No.62576346), the MOE Project of Key Research Institute of Humanities and Social Sciences (22JJD110001), the fundamental research funds for the central universities, and the research funds of Renmin University of China (24XNKJ13), and Beijing Advanced Innovation Center for Future Blockchain and Privacy Computing.

References

- [1] Alibaba. User behavior data from taobao for recommendation, 2018.
- [2] Emery N Brown, Riccardo Barbieri, Valérie Ventura, Robert E Kass, and Loren M Frank. The time-rescaling theorem and its application to neural spike train data analysis. *Neural computation*, 14(2):325–346, 2002.
- [3] Tianle Cai, Yuhong Li, Zhengyang Geng, Hongwu Peng, Jason D. Lee, Deming Chen, and Tri Dao. Medusa: Simple Ilm inference acceleration framework with multiple decoding heads. In Proceedings of the 41st International Conference on Machine Learning, ICML'24. JMLR.org, 2024.
- [4] George Casella, Christian P Robert, and Martin T Wells. Generalized accept-reject sampling schemes. *Lecture notes-monograph series*, pages 342–347, 2004.
- [5] Charlie Chen, Sebastian Borgeaud, Geoffrey Irving, Jean-Baptiste Lespiau, Laurent Sifre, and John Jumper. Accelerating large language model decoding with speculative sampling. *arXiv* preprint arXiv:2302.01318, 2023.
- [6] Daryl J Daley and David Vere-Jones. An introduction to the theory of point processes. vol. i. probability and its applications, 2003.
- [7] Nan Du, Hanjun Dai, Rakshit Trivedi, Utkarsh Upadhyay, Manuel Gomez-Rodriguez, and Le Song. Recurrent marked temporal point processes: embedding event history to vector. In *Proceedings of the 22nd ACM SIGKDD International Conference on Knowledge Discovery and Data Mining*, pages 1555–1564. ACM, 2016.
- [8] Nan Du, Hanjun Dai, Rakshit Trivedi, Utkarsh Upadhyay, Manuel Gomez-Rodriguez, and Le Song. Recurrent marked temporal point processes: Embedding event history to vector. In Balaji Krishnapuram, Mohak Shah, Alexander J. Smola, Charu C. Aggarwal, Dou Shen, and Rajeev Rastogi, editors, *Proceedings of the 22nd ACM SIGKDD International Conference on Knowledge Discovery and Data Mining, San Francisco, CA, USA, August 13-17, 2016*, pages 1555–1564. ACM, 2016.
- [9] Rémi Flamary, Nicolas Courty, Alexandre Gramfort, Mokhtar Z. Alaya, Aurélie Boisbunon, Stanislas Chambon, Laetitia Chapel, Adrien Corenflos, Kilian Fatras, Nemo Fournier, Léo Gautheron, Nathalie T.H. Gayraud, Hicham Janati, Alain Rakotomamonjy, Ievgen Redko, Antoine Rolet, Antony Schutz, Vivien Seguy, Danica J. Sutherland, Romain Tavenard, Alexander Tong, and Titouan Vayer. Pot: Python optimal transport. *Journal of Machine Learning Research*, 22(78):1–8, 2021.

- [10] Alan G Hawkes. Spectra of some self-exciting and mutually exciting point processes. *Biometrika*, 58(1):83–90, 1971.
- [11] Diederik P. Kingma and Jimmy Ba. Adam: A method for stochastic optimization, 2017.
- [12] John Frank Charles Kingman. *Poisson processes*, volume 3. Clarendon Press, 1992.
- [13] Donald E. Knuth. *The art of computer programming, volume 2 (3rd ed.): seminumerical algorithms.* Addison-Wesley Longman Publishing Co., Inc., USA, 1997.
- [14] Yaniv Leviathan, Matan Kalman, and Yossi Matias. Fast inference from transformers via speculative decoding. In *International Conference on Machine Learning*, pages 19274–19286. PMLR, 2023.
- [15] PA W Lewis and Gerald S Shedler. Simulation of nonhomogeneous poisson processes by thinning. *Naval research logistics quarterly*, 26(3):403–413, 1979.
- [16] Yuhui Li, Fangyun Wei, Chao Zhang, and Hongyang Zhang. Eagle: speculative sampling requires rethinking feature uncertainty. In *Proceedings of the 41st International Conference on Machine Learning*, ICML'24. JMLR.org, 2024.
- [17] Hongyuan Mei and Jason Eisner. The neural Hawkes process: A neurally self-modulating multivariate point process. In Isabelle Guyon, Ulrike von Luxburg, Samy Bengio, Hanna M. Wallach, Rob Fergus, S. V. N. Vishwanathan, and Roman Garnett, editors, Advances in Neural Information Processing Systems 30: Annual Conference on Neural Information Processing Systems 2017, December 4-9, 2017, Long Beach, CA, USA, pages 6754–6764, 2017.
- [18] Hongyuan Mei, Chenghao Yang, and Jason Eisner. Transformer embeddings of irregularly spaced events and their participants. In *International Conference on Learning Representations*, 2022.
- [19] Zizhuo Meng, Boyu Li, Xuhui Fan, Zhidong Li, Yang Wang, Fang Chen, and Feng Zhou. Transfeat-tpp: An interpretable deep covariate temporal point processes. In *ECAI*, 2024.
- [20] Zizhuo Meng, Ke Wan, Yadong Huang, Zhidong Li, Yang Wang, and Feng Zhou. Interpretable transformer hawkes processes: Unveiling complex interactions in social networks. In *Proceedings of the 30th ACM SIGKDD Conference on Knowledge Discovery and Data Mining*, pages 2200–2211, 2024.
- [21] Paul-André Meyer. Démonstration simplifiée d'un théorème de knight. Séminaire de probabilités de Strasbourg, 5:191–195, 1971.
- [22] Jianmo Ni, Jiacheng Li, and Julian McAuley. Justifying recommendations using distantly-labeled reviews and fine-grained aspects. In *Proceedings of the 2019 conference on empirical methods in natural language processing and the 9th international joint conference on natural language processing (EMNLP-IJCNLP)*, pages 188–197, 2019.
- [23] Yosihiko Ogata. On Lewis' simulation method for point processes. *IEEE Transactions on Information Theory*, 27(1):23–31, 1981.
- [24] Aristeidis Panos. Decomposable transformer point processes. In *Annual Conference on Neural Information Processing Systems*, 2024.
- [25] F Papangelou. Integrability of expected increments of point processes and a related random change of scale. *Transactions of the American Mathematical Society*, 165:483–506, 1972.
- [26] Razvan Pascanu, Tomas Mikolov, and Yoshua Bengio. On the difficulty of training recurrent neural networks. In *Proceedings of the 30th International Conference on International Conference on Machine Learning-Volume* 28, pages III–1310, 2013.
- [27] Reiner Pope, Sholto Douglas, Aakanksha Chowdhery, Jacob Devlin, James Bradbury, Jonathan Heek, Kefan Xiao, Shivani Agrawal, and Jeff Dean. Efficiently scaling transformer inference. *Proceedings of Machine Learning and Systems*, 5:606–624, 2023.

- [28] Jakob Gulddahl Rasmussen. Lecture notes: Temporal point processes and the conditional intensity function, 2018.
- [29] Oleksandr Shchur, Marin Bilos, and Stephan Günnemann. Intensity-free learning of temporal point processes. In 8th International Conference on Learning Representations, ICLR 2020, Addis Ababa, Ethiopia, April 26-30, 2020. OpenReview.net, 2020.
- [30] Oleksandr Shchur, Nicholas Gao, Marin Biloš, and Stephan Günnemann. Fast and flexible temporal point processes with triangular maps. *Advances in Neural Information Processing Systems*, 33:73–84, 2020.
- [31] Qingmei Wang, Minjie Cheng, Shen Yuan, and Hongteng Xu. Hierarchical contrastive learning for temporal point processes. *Proceedings of the AAAI Conference on Artificial Intelligence*, 37(8):10166–10174, Jun. 2023.
- [32] Zili Wang, Robert Zhang, Kun Ding, Qi Yang, Fei Li, and Shiming Xiang. Continuous speculative decoding for autoregressive image generation, 2024.
- [33] Chris Whong. Foiling nyc's taxi trip data. https://chriswhong.com/open-data/foil_nyc_taxi/, 2014.
- [34] Siqiao Xue, Xiaoming Shi, Zhixuan Chu, Yan Wang, Hongyan Hao, Fan Zhou, Caigao Jiang, Chen Pan, James Y. Zhang, Qingsong Wen, Jun Zhou, and Hongyuan Mei. Easytpp: Towards open benchmarking temporal point processes. In *International Conference on Learning Representations (ICLR)*, 2024.
- [35] Siqiao Xue, Xiaoming Shi, Y James Zhang, and Hongyuan Mei. Hypro: A hybridly normalized probabilistic model for long-horizon prediction of event sequences. In *Advances in Neural Information Processing Systems*, 2022.
- [36] Qiang Zhang, Aldo Lipani, Ömer Kirnap, and Emine Yilmaz. Self-attentive Hawkes process. In *Proceedings of the 37th International Conference on Machine Learning, ICML 2020, 13-18 July 2020, Virtual Event*, volume 119 of *Proceedings of Machine Learning Research*, pages 11183–11193. PMLR, 2020.
- [37] Feng Zhou, Quyu Kong, Zhijie Deng, Jichao Kan, Yixuan Zhang, Cheng Feng, and Jun Zhu. Efficient inference for dynamic flexible interactions of neural populations. *Journal of Machine Learning Research*, 23(211):1–49, 2022.
- [38] Feng Zhou, Quyu Kong, and Yixuan Zhang. Advances in temporal point processes: Bayesian, deep, and Ilm approaches. *arXiv* preprint arXiv:2501.14291, 2025.
- [39] Feng Zhou, Zhidong Li, Xuhui Fan, Yang Wang, Arcot Sowmya, and Fang Chen. Efficient inference for nonparametric Hawkes processes using auxiliary latent variables. *Journal of Machine Learning Research*, 21(241):1–31, 2020.
- [40] Simiao Zuo, Haoming Jiang, Zichong Li, Tuo Zhao, and Hongyuan Zha. Transformer Hawkes process. In Proceedings of the 37th International Conference on Machine Learning, ICML 2020, 13-18 July 2020, Virtual Event, volume 119 of Proceedings of Machine Learning Research, pages 11692–11702. PMLR, 2020.

NeurIPS Paper Checklist

1. Claims

Question: Do the main claims made in the abstract and introduction accurately reflect the paper's contributions and scope?

Answer: [Yes]

Justification: The main claims made in the abstract and introduction accurately reflect the paper's contributions and scope. See the Abstract and Introduction sections.

Guidelines:

- The answer NA means that the abstract and introduction do not include the claims made in the paper.
- The abstract and/or introduction should clearly state the claims made, including the contributions made in the paper and important assumptions and limitations. A No or NA answer to this question will not be perceived well by the reviewers.
- The claims made should match theoretical and experimental results, and reflect how much the results can be expected to generalize to other settings.
- It is fine to include aspirational goals as motivation as long as it is clear that these goals are not attained by the paper.

2. Limitations

Question: Does the paper discuss the limitations of the work performed by the authors?

Answer: [Yes]

Justification: The limitation of the work is discussed in the appendix.

Guidelines:

- The answer NA means that the paper has no limitation while the answer No means that the paper has limitations, but those are not discussed in the paper.
- The authors are encouraged to create a separate "Limitations" section in their paper.
- The paper should point out any strong assumptions and how robust the results are to violations of these assumptions (e.g., independence assumptions, noiseless settings, model well-specification, asymptotic approximations only holding locally). The authors should reflect on how these assumptions might be violated in practice and what the implications would be.
- The authors should reflect on the scope of the claims made, e.g., if the approach was only tested on a few datasets or with a few runs. In general, empirical results often depend on implicit assumptions, which should be articulated.
- The authors should reflect on the factors that influence the performance of the approach. For example, a facial recognition algorithm may perform poorly when image resolution is low or images are taken in low lighting. Or a speech-to-text system might not be used reliably to provide closed captions for online lectures because it fails to handle technical jargon.
- The authors should discuss the computational efficiency of the proposed algorithms and how they scale with dataset size.
- If applicable, the authors should discuss possible limitations of their approach to address problems of privacy and fairness.
- While the authors might fear that complete honesty about limitations might be used by reviewers as grounds for rejection, a worse outcome might be that reviewers discover limitations that aren't acknowledged in the paper. The authors should use their best judgment and recognize that individual actions in favor of transparency play an important role in developing norms that preserve the integrity of the community. Reviewers will be specifically instructed to not penalize honesty concerning limitations.

3. Theory assumptions and proofs

Question: For each theoretical result, does the paper provide the full set of assumptions and a complete (and correct) proof?

Answer: [Yes]

Justification: For all theoretical results, the paper provides the corresponding proofs in the appendix.

Guidelines:

- The answer NA means that the paper does not include theoretical results.
- All the theorems, formulas, and proofs in the paper should be numbered and cross-referenced.
- All assumptions should be clearly stated or referenced in the statement of any theorems.
- The proofs can either appear in the main paper or the supplemental material, but if they appear in the supplemental material, the authors are encouraged to provide a short proof sketch to provide intuition.
- Inversely, any informal proof provided in the core of the paper should be complemented by formal proofs provided in appendix or supplemental material.
- Theorems and Lemmas that the proof relies upon should be properly referenced.

4. Experimental result reproducibility

Question: Does the paper fully disclose all the information needed to reproduce the main experimental results of the paper to the extent that it affects the main claims and/or conclusions of the paper (regardless of whether the code and data are provided or not)?

Answer: [Yes]

Justification: The paper fully discloses all the information needed to reproduce the main experimental results in the paper. See the Experiments section.

Guidelines:

- The answer NA means that the paper does not include experiments.
- If the paper includes experiments, a No answer to this question will not be perceived
 well by the reviewers: Making the paper reproducible is important, regardless of
 whether the code and data are provided or not.
- If the contribution is a dataset and/or model, the authors should describe the steps taken to make their results reproducible or verifiable.
- Depending on the contribution, reproducibility can be accomplished in various ways. For example, if the contribution is a novel architecture, describing the architecture fully might suffice, or if the contribution is a specific model and empirical evaluation, it may be necessary to either make it possible for others to replicate the model with the same dataset, or provide access to the model. In general, releasing code and data is often one good way to accomplish this, but reproducibility can also be provided via detailed instructions for how to replicate the results, access to a hosted model (e.g., in the case of a large language model), releasing of a model checkpoint, or other means that are appropriate to the research performed.
- While NeurIPS does not require releasing code, the conference does require all submissions to provide some reasonable avenue for reproducibility, which may depend on the nature of the contribution. For example
 - (a) If the contribution is primarily a new algorithm, the paper should make it clear how to reproduce that algorithm.
- (b) If the contribution is primarily a new model architecture, the paper should describe the architecture clearly and fully.
- (c) If the contribution is a new model (e.g., a large language model), then there should either be a way to access this model for reproducing the results or a way to reproduce the model (e.g., with an open-source dataset or instructions for how to construct the dataset).
- (d) We recognize that reproducibility may be tricky in some cases, in which case authors are welcome to describe the particular way they provide for reproducibility. In the case of closed-source models, it may be that access to the model is limited in some way (e.g., to registered users), but it should be possible for other researchers to have some path to reproducing or verifying the results.

5. Open access to data and code

Question: Does the paper provide open access to the data and code, with sufficient instructions to faithfully reproduce the main experimental results, as described in supplemental material?

Answer: [Yes]

Justification: We provide the data and code in the supplemental material to reproduce the main experimental results.

Guidelines:

- The answer NA means that paper does not include experiments requiring code.
- Please see the NeurIPS code and data submission guidelines (https://nips.cc/public/guides/CodeSubmissionPolicy) for more details.
- While we encourage the release of code and data, we understand that this might not be possible, so "No" is an acceptable answer. Papers cannot be rejected simply for not including code, unless this is central to the contribution (e.g., for a new open-source benchmark).
- The instructions should contain the exact command and environment needed to run to reproduce the results. See the NeurIPS code and data submission guidelines (https://nips.cc/public/guides/CodeSubmissionPolicy) for more details.
- The authors should provide instructions on data access and preparation, including how
 to access the raw data, preprocessed data, intermediate data, and generated data, etc.
- The authors should provide scripts to reproduce all experimental results for the new proposed method and baselines. If only a subset of experiments are reproducible, they should state which ones are omitted from the script and why.
- At submission time, to preserve anonymity, the authors should release anonymized versions (if applicable).
- Providing as much information as possible in supplemental material (appended to the paper) is recommended, but including URLs to data and code is permitted.

6. Experimental setting/details

Question: Does the paper specify all the training and test details (e.g., data splits, hyper-parameters, how they were chosen, type of optimizer, etc.) necessary to understand the results?

Answer: [Yes]

Justification: We specify all the training and test details necessary to understand the results. See the Experiments section.

Guidelines:

- The answer NA means that the paper does not include experiments.
- The experimental setting should be presented in the core of the paper to a level of detail that is necessary to appreciate the results and make sense of them.
- The full details can be provided either with the code, in appendix, or as supplemental material.

7. Experiment statistical significance

Question: Does the paper report error bars suitably and correctly defined or other appropriate information about the statistical significance of the experiments?

Answer: [Yes]

Justification: We report the statistical significance of the experiments. In the figures presenting the experimental results, we provide the standard deviations across multiple runs.

- The answer NA means that the paper does not include experiments.
- The authors should answer "Yes" if the results are accompanied by error bars, confidence intervals, or statistical significance tests, at least for the experiments that support the main claims of the paper.

- The factors of variability that the error bars are capturing should be clearly stated (for example, train/test split, initialization, random drawing of some parameter, or overall run with given experimental conditions).
- The method for calculating the error bars should be explained (closed form formula, call to a library function, bootstrap, etc.)
- The assumptions made should be given (e.g., Normally distributed errors).
- It should be clear whether the error bar is the standard deviation or the standard error
 of the mean.
- It is OK to report 1-sigma error bars, but one should state it. The authors should preferably report a 2-sigma error bar than state that they have a 96% CI, if the hypothesis of Normality of errors is not verified.
- For asymmetric distributions, the authors should be careful not to show in tables or figures symmetric error bars that would yield results that are out of range (e.g. negative error rates).
- If error bars are reported in tables or plots, The authors should explain in the text how they were calculated and reference the corresponding figures or tables in the text.

8. Experiments compute resources

Question: For each experiment, does the paper provide sufficient information on the computer resources (type of compute workers, memory, time of execution) needed to reproduce the experiments?

Answer: [Yes]

Justification: All experiments are conducted on the server whose details are provided in the paper. See the Experiments section.

Guidelines:

- The answer NA means that the paper does not include experiments.
- The paper should indicate the type of compute workers CPU or GPU, internal cluster, or cloud provider, including relevant memory and storage.
- The paper should provide the amount of compute required for each of the individual experimental runs as well as estimate the total compute.
- The paper should disclose whether the full research project required more compute than the experiments reported in the paper (e.g., preliminary or failed experiments that didn't make it into the paper).

9. Code of ethics

Question: Does the research conducted in the paper conform, in every respect, with the NeurIPS Code of Ethics https://neurips.cc/public/EthicsGuidelines?

Answer: [Yes]

Justification: The research conducted in the paper conform with the NeurIPS Code of Ethics. Guidelines:

- The answer NA means that the authors have not reviewed the NeurIPS Code of Ethics.
- If the authors answer No, they should explain the special circumstances that require a
 deviation from the Code of Ethics.
- The authors should make sure to preserve anonymity (e.g., if there is a special consideration due to laws or regulations in their jurisdiction).

10. Broader impacts

Question: Does the paper discuss both potential positive societal impacts and negative societal impacts of the work performed?

Answer: [No]

Justification: This paper presents work whose goal is to advance the field of machine learning. There are many potential societal consequences of our work, none of which we feel must be specifically highlighted here.

- The answer NA means that there is no societal impact of the work performed.
- If the authors answer NA or No, they should explain why their work has no societal impact or why the paper does not address societal impact.
- Examples of negative societal impacts include potential malicious or unintended uses (e.g., disinformation, generating fake profiles, surveillance), fairness considerations (e.g., deployment of technologies that could make decisions that unfairly impact specific groups), privacy considerations, and security considerations.
- The conference expects that many papers will be foundational research and not tied to particular applications, let alone deployments. However, if there is a direct path to any negative applications, the authors should point it out. For example, it is legitimate to point out that an improvement in the quality of generative models could be used to generate deepfakes for disinformation. On the other hand, it is not needed to point out that a generic algorithm for optimizing neural networks could enable people to train models that generate Deepfakes faster.
- The authors should consider possible harms that could arise when the technology is being used as intended and functioning correctly, harms that could arise when the technology is being used as intended but gives incorrect results, and harms following from (intentional or unintentional) misuse of the technology.
- If there are negative societal impacts, the authors could also discuss possible mitigation strategies (e.g., gated release of models, providing defenses in addition to attacks, mechanisms for monitoring misuse, mechanisms to monitor how a system learns from feedback over time, improving the efficiency and accessibility of ML).

11. Safeguards

Question: Does the paper describe safeguards that have been put in place for responsible release of data or models that have a high risk for misuse (e.g., pretrained language models, image generators, or scraped datasets)?

Answer: [NA]

Justification: The paper poses no such risks.

Guidelines:

- The answer NA means that the paper poses no such risks.
- Released models that have a high risk for misuse or dual-use should be released with
 necessary safeguards to allow for controlled use of the model, for example by requiring
 that users adhere to usage guidelines or restrictions to access the model or implementing
 safety filters.
- Datasets that have been scraped from the Internet could pose safety risks. The authors should describe how they avoided releasing unsafe images.
- We recognize that providing effective safeguards is challenging, and many papers do not require this, but we encourage authors to take this into account and make a best faith effort.

12. Licenses for existing assets

Question: Are the creators or original owners of assets (e.g., code, data, models), used in the paper, properly credited and are the license and terms of use explicitly mentioned and properly respected?

Answer: [Yes]

Justification: All code, models, and datasets mentioned in the text are appropriately cited with their original papers.

- The answer NA means that the paper does not use existing assets.
- The authors should cite the original paper that produced the code package or dataset.
- The authors should state which version of the asset is used and, if possible, include a URL.
- The name of the license (e.g., CC-BY 4.0) should be included for each asset.

- For scraped data from a particular source (e.g., website), the copyright and terms of service of that source should be provided.
- If assets are released, the license, copyright information, and terms of use in the
 package should be provided. For popular datasets, paperswithcode.com/datasets
 has curated licenses for some datasets. Their licensing guide can help determine the
 license of a dataset.
- For existing datasets that are re-packaged, both the original license and the license of the derived asset (if it has changed) should be provided.
- If this information is not available online, the authors are encouraged to reach out to the asset's creators.

13. New assets

Question: Are new assets introduced in the paper well documented and is the documentation provided alongside the assets?

Answer: [Yes]

Justification: New assets introduced in the paper, such as code, are well documented. The documentation is provided alongside the assets in the supplementary material.

Guidelines:

- The answer NA means that the paper does not release new assets.
- Researchers should communicate the details of the dataset/code/model as part of their submissions via structured templates. This includes details about training, license, limitations, etc.
- The paper should discuss whether and how consent was obtained from people whose asset is used.
- At submission time, remember to anonymize your assets (if applicable). You can either create an anonymized URL or include an anonymized zip file.

14. Crowdsourcing and research with human subjects

Question: For crowdsourcing experiments and research with human subjects, does the paper include the full text of instructions given to participants and screenshots, if applicable, as well as details about compensation (if any)?

Answer: [NA]

Justification: The paper does not involve crowdsourcing nor research with human subjects. Guidelines:

- The answer NA means that the paper does not involve crowdsourcing nor research with human subjects.
- Including this information in the supplemental material is fine, but if the main contribution of the paper involves human subjects, then as much detail as possible should be included in the main paper.
- According to the NeurIPS Code of Ethics, workers involved in data collection, curation, or other labor should be paid at least the minimum wage in the country of the data collector.

15. Institutional review board (IRB) approvals or equivalent for research with human subjects

Question: Does the paper describe potential risks incurred by study participants, whether such risks were disclosed to the subjects, and whether Institutional Review Board (IRB) approvals (or an equivalent approval/review based on the requirements of your country or institution) were obtained?

Answer: [NA]

Justification: The paper does not involve crowdsourcing nor research with human subjects. Guidelines:

 The answer NA means that the paper does not involve crowdsourcing nor research with human subjects.

- Depending on the country in which research is conducted, IRB approval (or equivalent) may be required for any human subjects research. If you obtained IRB approval, you should clearly state this in the paper.
- We recognize that the procedures for this may vary significantly between institutions and locations, and we expect authors to adhere to the NeurIPS Code of Ethics and the guidelines for their institution.
- For initial submissions, do not include any information that would break anonymity (if applicable), such as the institution conducting the review.

16. Declaration of LLM usage

Question: Does the paper describe the usage of LLMs if it is an important, original, or non-standard component of the core methods in this research? Note that if the LLM is used only for writing, editing, or formatting purposes and does not impact the core methodology, scientific rigorousness, or originality of the research, declaration is not required.

Answer: [NA]

Justification: The core method development in this research does not involve LLMs as any important, original, or non-standard components.

- The answer NA means that the core method development in this research does not involve LLMs as any important, original, or non-standard components.
- Please refer to our LLM policy (https://neurips.cc/Conferences/2025/LLM) for what should or should not be described.

A Proof of Mathematical Theorems

A.1 Sampling from a Log-Normal Mixture Model

To sample a random variable τ from a log-normal mixture distribution where w_m are the mixture weights, μ_m are the location parameters and σ_m are the scale parameters, M is the number of mixture components

$$p(\tau) = \sum_{m=1}^{M} w_m \cdot \frac{1}{\tau \sqrt{2\pi\sigma_m^2}} \exp\left(-\frac{(\log \tau - \mu_m)^2}{2\sigma_m^2}\right),\tag{5}$$

we only need to do the following procedure

$$z \sim \text{Categorical}(w_1, \dots, w_M), \ \epsilon \in \mathcal{N}(0, 1), \ \tau = \exp(\mu_z + \sigma_z \cdot \epsilon),$$
 (6)

where z is a single integer $z \in \{1,\ldots,M\}$. By $z \sim \text{Categorical}(w_1,\ldots,w_M)$, we choose the z-th mode of the mixture of log-normal with location and scale parameter (μ_z,σ_z) . Then by using the change-of-variable formula

$$p(\tau) = p(\epsilon) \left| \frac{\mathrm{d}\epsilon}{\mathrm{d}\tau} \right| = \frac{1}{\sqrt{2\pi}} \cdot \exp\left(-\frac{(\log \tau - \mu_z)^2}{2\sigma_z^2}\right) \frac{1}{\sigma_z \tau} = \frac{1}{\tau \sqrt{2\pi}\sigma_z} \exp\left(-\frac{(\log \tau - \mu_z)^2}{2\sigma_z^2}\right),$$
(7)

which is exactly the PDF of $\mathcal{LN}(\mu_z, \sigma_z)$.

A.2 Correctness of Sampling from the Adjusted Distribution

Denote β_{τ} as the acceptance probability of candidate event interval in SD, i.e.

$$\beta_{\tau} = \mathbb{E}_{\tau \sim g_D(\tau_{i+l}|\cdot)} \min\left(1, \frac{g_T(\tau_{i+l}|\cdot)}{g_D(\tau_{i+l}|\cdot)}\right) = \int \min\left(g_T(\tau|\cdot), g_D(\tau|\cdot)\right) d\tau. \tag{8}$$

Note that

$$g'(\tau_{i+l}|\cdot) = \frac{\max(0, g_T(\tau_{i+l}|\cdot) - g_D(\tau_{i+l}|\cdot))}{\int \max(0, g_T(\tau_{i+l}|\cdot) - g_D(\tau_{i+l}|\cdot)) d\tau_{i+l}} = \frac{g_T(\tau_{i+l}|\cdot) - \min(g_D(\tau_{i+l}|\cdot), g_T(\tau_{i+l}|\cdot))}{1 - \beta_\tau}$$
(9)

Denote $P(\text{accept}, \tau')$ as the probability that the sample τ' drawn by the draft model is accepted by the target model, and $P(\text{reject}, \tau')$ as the probability that τ' is rejected and subsequently resampled from the adjusted distribution defined in Eq. (3). By the law of total probability, the distribution of a sample τ' drawn by SD can be calculated as

$$p(\tau') = P(\text{accept}, \tau') + P(\text{reject}, \tau')$$
(10)

$$= \min\left(1, \frac{g_T(\tau'|\cdot)}{g_D(\tau'|\cdot)}\right) g_D(\tau'|\cdot) + (1 - \beta_\tau)g'(\tau'|\cdot)$$
(11)

$$= \min\left(1, \frac{g_T(\tau'|\cdot)}{g_D(\tau'|\cdot)}\right) g_D(\tau'|\cdot) + \left(g_T(\tau'|\cdot) - \min(g_D(\tau'|\cdot), g_T(\tau'|\cdot))\right) \tag{12}$$

$$=g_T(\tau'|\cdot). \tag{13}$$

which justifies the correctness of sampling from an adjusted distribution. The derivation also shows that sampling τ' directly from the target distribution $g_T(\tau_{i+L}|\cdot)$ instead of the adjusted distribution $g'(\tau_{i+L}|\cdot)$ after rejection would result in $p(\tau') \neq g_T(\tau'|\cdot)$, leading to incorrect sampling. Similarly, denote the acceptance probability of candidate event type in SD as $\beta_k = \mathbb{E}_{k \sim f_D(k_{i+l}|\cdot)} \min\left(1, \frac{f_T(k_{i+l}|\cdot)}{f_D(k_{i+l}|\cdot)}\right) = \sum_k \min\left(f_T(k|\cdot), f_D(k|\cdot)\right)$, we can also derive the correctness of sampling $k' \sim f'(k_{i+l}|\cdot)$:

$$p(k') = P(\text{accept}, k') + P(\text{reject}, k')$$
(14)

$$= \min\left(1, \frac{f_T(k'|\cdot)}{f_D(k'|\cdot)}\right) f_D(k'|\cdot) + (1 - \beta_k) f'(k'|\cdot) \tag{15}$$

$$= \min\left(1, \frac{f_T(k'|\cdot)}{f_D(k'|\cdot)}\right) f_D(k'|\cdot) + (f_T(k'|\cdot) - \min(f_D(k'|\cdot), f_T(k'|\cdot)))$$
(16)

$$= f_T(k'|\cdot). \tag{17}$$

A.3 Proof of Theorem 1

We refer to [32] for the proof in this subsection. We begin by recalling the principle and demonstrating the correctness of the standard acceptance-rejection sampling [4], which aims to draw samples from a target distribution $p(\tau)$ using a proposal distribution $q(\tau)$ such that $p(\tau) \leq Mq(\tau)$, $\forall \tau \in \mathcal{T}$, where \mathcal{T} is the support of $p(\tau)$ and $p(\tau)$, and $p(\tau)$ and $p(\tau)$ are a finite constant. The procedure is as follows: (1) Sample a candidate $\hat{\tau} = q(\tau)$. (2) Sample a uniform random variable $\epsilon \sim \text{Uniform}(0,1)$. (3) Accept the candidate $\hat{\tau}$ if $\epsilon < \frac{p(\hat{\tau})}{Mq(\hat{\tau})}$; otherwise, reject it and return to step (1). To prove that the accepted samples follow the distribution $p(\tau)$, let \mathcal{A} be any measurable set within the support \mathcal{T} . The probability that an accepted sample $\hat{\tau}$ falls into \mathcal{A} is

$$\mathbb{P}(\hat{\tau} \in \mathcal{A}|\hat{\tau} \text{ is accepted}) = \frac{\mathbb{P}(\hat{\tau} \in \mathcal{A}, \hat{\tau} \text{ is accepted})}{\mathbb{P}(\hat{\tau} \text{ is accepted})} = \frac{\mathbb{P}(\hat{\tau} \in \mathcal{A}, \hat{\tau} \text{ is accepted})}{\mathbb{P}(\hat{\tau} \in \mathcal{T}, \hat{\tau} \text{ is accepted})}.$$
 (18)

Note that

$$\mathbb{P}(\hat{\tau} \in \mathcal{A}, \hat{\tau} \text{ is accepted}) = \int_{\mathcal{T}} \int_{0}^{1} \mathbb{I}(\hat{\tau} \in \mathcal{A}) \mathbb{I}\left(\epsilon < \frac{p(\hat{\tau})}{Mq(\hat{\tau})}\right) p(\hat{\tau}) d\epsilon d\hat{\tau}$$
(19)

$$= \frac{1}{M} \int_{\mathcal{T}} \mathbb{I}(\hat{\tau} \in \mathcal{A}) \frac{p(\hat{\tau})}{q(\hat{\tau})} q(\hat{\tau}) d\hat{\tau} = \frac{1}{M} \int_{\mathcal{A}} p(\hat{\tau}) d\hat{\tau}.$$
 (20)

Therefore,

$$\mathbb{P}(\hat{\tau} \in \mathcal{A} | \hat{\tau} \text{ is accepted}) = \frac{\int_{\mathcal{A}} p(\hat{\tau}) d\hat{\tau} / M}{\int_{\mathcal{T}} p(\hat{\tau}) d\hat{\tau} / M} = \int_{\mathcal{A}} p(\hat{\tau}) d\hat{\tau}, \tag{21}$$

which justifies the correctness of acceptance-rejection sampling. Now we apply this acceptance-rejection sampling framework to the specific scenario described in the theorem. The adjusted distribution $g'(\tau_{i+l}|\cdot)$ defined in Eq. (3) corresponds to the target distribution $p(\tau)$, and $g_T(\tau_{i+l}|\cdot)$ corresponds to the proposal distribution $q(\tau)$. We need to find the constant M such that for any sampled $\hat{\tau}_{i+L}$, $g'(\hat{\tau}_{i+l}|\cdot) \leq Mg_T(\hat{\tau}_{i+l}|\cdot)$. Denote $Z = \int \max\left(0, g_T(\hat{\tau}_{i+l}|\cdot) - g_D(\hat{\tau}_{i+l}|\cdot)\right) \mathrm{d}\hat{\tau}_{i+l}$, note that

$$g'(\hat{\tau}_{i+l}|\cdot) = \frac{\max(0, g_T(\hat{\tau}_{i+l}|\cdot) - g_D(\hat{\tau}_{i+l}|\cdot))}{Z} \le \frac{g_T(\hat{\tau}_{i+l}|\cdot) - g_D(\hat{\tau}_{i+l}|\cdot)}{Z} \le \frac{g_T(\hat{\tau}_{i+l}|\cdot)}{Z}, \quad (22)$$

This inequality confirms that we can set M:=1/Z to satisfy the requirement of acceptance-rejection sampling. With $M=\frac{1}{Z}$, the acceptance threshold α is computed as

$$\alpha = \frac{g'(\hat{\tau}_{i+l}|\cdot)}{Mg_T(\hat{\tau}_{i+l}|\cdot)} = \frac{\max(0, g_T(\hat{\tau}_{i+l}|\cdot) - g_D(\hat{\tau}_{i+l}|\cdot))/Z}{g_T(\hat{\tau}_{i+l}|\cdot)/Z} = \frac{\max(0, g_T(\hat{\tau}_{i+l}|\cdot) - g_D(\hat{\tau}_{i+l}|\cdot))}{g_T(\hat{\tau}_{i+l}|\cdot)}.$$
(23)

which is precisely the acceptance threshold α defined in Theorem 1.

A.4 Computation of the KS Statistic

We employ the Kolmogorov-Smirnov (KS) statistic to assess whether sampled realizations conform to ground truth distributions in synthetic point processes. For n i.i.d. ordered observations $\{X_i\}_{i=1}^n$ from a distribution F(x), the KS statistic is defined as $D_{KS} = \sup_x |F_n(x) - F(x)|$, where $F_n(x)$ is the empirical cumulative distribution of $\{X_i\}_{i=1}^n$. The leverage of KS statistic is guaranteed by Theorem 2.

Theorem 2 (Time Rescaling Theorem [21, 25]). Given a point process with CIF $\lambda(t|\mathcal{H}_t)$ and with occurrence times $0 < t_1 < \cdots < t_n \leq T$, define

$$z_1 = \int_0^{t_1} \lambda(t|\mathcal{H}_t) dt, \ z_i = \int_{t_{i-1}}^{t_i} \lambda(t|\mathcal{H}_t) dt, \ i = 2, \dots, n.$$
 (24)

Then $\{z_i\}_{i=1}^n$ are independent exponential random variables with rate parameter 1.

By transforming sampled timestamps $\{t_i\}_{i=1}^n$ using the ground truth intensity function, we obtain rescaled intervals $\{z_i\}_{i=1}^n$ whose empirical distribution $F_n(x)$ should approximate $F(x) = 1 - e^{-x}$, x > 0 if sampling is correct. Low $D_{\rm KS}$ values indicate high conformity to the ground truth distribution.

B Dataset Statistics

B.1 Synthetic Dataset

We consider three sets of synthetic data, where each dataset contains 1000 sequences and is split into 80%/10%/10% for training/validation/testing. The data are simulated using the traditional thinning algorithm [15, 23].

Poisson is simulated from an inhomogeneous Poisson process with an intensity function $\lambda(t) = A\left(b + \sin\left(\omega\pi t\right)\right)$ with $A = 5, b = 1, \omega = \frac{1}{50}$ and time span T = 100.

Hawkes is simulated from a single-variate Hawkes process $\lambda(t) = \mu + \sum_{t_i < t} \alpha \exp(-\beta(t - t_i))$ with $\mu = 2.5, \alpha = 1, \beta = 2$ and time span T = 100.

Multi-Hawkes is simulated from a M-dimensional Hawkes process, where the intensity for the j-th dimension is $\lambda_j(t) = \mu_m + \sum_{i=1}^M \sum_{\substack{t_i^j < t \\ i}} \alpha_{ij} \exp(-\beta_{ij}(t-t_i^j))$. Here $M=2, \mu_1=\mu_2=0.4, \alpha_{11}=\alpha_{22}=1, \alpha_{12}=0.5, \alpha_{21}=0.1, \beta_{11}=\beta_{12}=\beta_{21}=\beta_{22}=2$.

B.2 Real Dataset

We consider four sets of real data listed below. For all datasets, we maintained the standard training/validation/testing splits established in prior work.

Taobao [1] captures the temporal behavioral patterns of the 2,000 most engaged anonymous users on the Taobao e-commerce platform during a nine-day period from November 25th to December 3rd, 2017. The dataset encompasses K=17 distinct event categories.

Amazon [22] documents the chronological shopping activities of anonymous customers on the Amazon marketplace from January 2008 to October 2018. The dataset features K=16 different event categories that characterize various user interactions with the platform.

Taxi [33] comprises pickup and dropoff incidents for taxis operating across New York City's five boroughs (Manhattan, Brooklyn, Queens, The Bronx, and Staten Island). Each borough-specific pickup or dropoff action is classified as a distinct event type, yielding a total of K=10 event categories.

StackOverflow [8] consists of sequential badge-earning events by users on the prominent question-answering platform StackOverflow. Individual users accumulate various badges over approximately a two-year timeframe, with the dataset containing K=22 unique badge types in total.

C Addtional Experiment Details

C.1 Algorithm for TPP-SD

The pseudo code for the algorithm of TPP-SD is shown in Algorithm 1.

C.2 Training Details

To implement our proposed CDF-based Transformer TPP model, we modified the codebase from [29]. The original RNN encoder for history aggregation was replaced with Transformer backbones proposed by THP [40], SAHP [36], and AttNHP [18]. Given that these models are CIF-based, we extracted only their Transformer architectures, utilizing implementations available in the EasyTPP [34] GitHub repository³. In line with [29], we set the history embedding dimension D=64 and the number of mixture components M=64.

³https://github.com/ant-research/EasyTemporalPointProcess

Algorithm 1: TPP-SD

```
1 Inputs: Initial event (t_0, k_0), end time T, number of draft events \gamma, target model
       \mathcal{M}_T = \{\mathcal{E}_T, g_T(\tau|\cdot), f_T(k|\cdot)\}, \text{ draft model } \mathcal{M}_D = \{\mathcal{E}_D, g_D(\tau|\cdot), f_D(k|\cdot)\};
 2 Initialize: Sampled events S = \{(t_0, k_0)\}, i \leftarrow 0;
 3 while t_i < T do
             for l=1 to \gamma do
 4
                    Sample \hat{\tau}_{i+l} \sim g_D(\tau|\cdot), record g_D(\hat{\tau}_{i+l}|\cdot) and \hat{t}_{i+l} \leftarrow t_{i+l-1} + \hat{\tau}_{i+l};
 5
                    Sample \hat{k}_{i+l} \sim f_D(k|\cdot) and record f_D(\hat{k}_{i+l}|\cdot);
 6
             Compute g_T(\hat{\tau}_{i+1}|\cdot), \dots, g_T(\hat{\tau}_{i+\gamma}|\cdot) and f_T(\hat{k}_{i+1}|\cdot), \dots, f_T(\hat{k}_{i+\gamma}|\cdot) in parallel;
 7
            \epsilon_1^{\tau}, \dots \epsilon_{\gamma}^{\tau}, \epsilon_1^{k}, \dots, \epsilon_{\gamma}^{k} \sim \text{Uniform}(0, 1);
            L \leftarrow \{\min(l_1, l_2) | 1 \leq l_1, l_2 \leq \gamma, \epsilon_{l_1}^{\tau} > \frac{g_T(\hat{\tau}_{i+l_1}|\cdot)}{g_D(\hat{\tau}_{i+l_1}|\cdot)}, \epsilon_{l_2}^{k} > \frac{f_T(\hat{k}_{i+l_2}|\cdot)}{f_D(\hat{k}_{i+l_2}|\cdot)}\};
10
                    Sample \hat{\tau}_{i+L} \sim g'(\tau_{i+L}|\cdot) and \hat{t}_{i+L} = t_{i+L-1} + \hat{\tau}_{i+L};
11
                 Sample \hat{k}_{i+L} \sim f'(k_{i+L}|\cdot);
12
             S \leftarrow S \cup \{(\hat{t}_{i+1}, \hat{k}_{i+1}), \dots, (\hat{t}_{i+L}, \hat{k}_{i+L})\};
13
             i \leftarrow i + L;
14
16 \mathcal{S} \leftarrow \{(t_i, k_i) \mid (t_i, k_i) \in \mathcal{S}, t_i \leq T\};
17 Return: S
```

By default, we trained an 8-head, 20-layer target model and a 1-head, 1-layer draft model for each dataset. All models were trained using the Adam optimizer [11] for up to 1000 epochs with a batch size of 16 on one single NVIDIA RTX 4090. Early stopping based on validation log-likelihood was applied to prevent overfitting.

C.3 Sampling Details

C.3.1 Sampling Synthetic TPPs

For the experiments in Section 5.2, we evaluate sampling performance within the time window [0,100]. We report the discrepancy metrics $\Delta \mathcal{L}_{\rm ar}^{\rm syn}$ and $\Delta \mathcal{L}_{\rm sd}^{\rm syn}$, the KS statistics $D_{\rm KS}$, the execution time $T_{\rm AR}$ and $T_{\rm SD}$, and the resulting speedup ratio $S_{\rm AR/SD}$ as defined in Section 5.1. We conducted experiments across three random seeds and report the mean for each metric to ensure result robustness.

Apart from numerical metrics, we employ Kolmogorov-Smirnov plots (KS plots) to visualize sampling quality, which compare the empirical cumulative distribution $F_n(x)$ of the rescaled intervals $\{z_i\}_{i=1}^n$ against the theoretical cumulative distribution $F(x) = 1 - e^{-x}$ given by [2]. The KS plot visualizes points $\{(F(z_i), F_n(z_i))\}_{i=1}^n$, where perfect sampling would yield points along the 45-degree line.

We conduct formal statistical assessment using the Kolmogorov-Smirnov test with the following hypotheses:

$$H_0: F_n(x) = F(x)$$
 versus $H_1: F_n(x) \neq F(x)$, (25)

Reject
$$H_0$$
 if: $D_{KS} > \frac{c(\alpha)}{\sqrt{n}}$, (26)

where n is the number of sampled events, $D_{\rm KS}=\sup_x|F_n(x)-F(x)|$ is the KS statistic, and $c(\alpha)=1.36$ at significance level $\alpha=0.05$ [13]. Based on this test, we construct a 95% confidence band $CB=\{(F(x),y):y\in [F(x)-\frac{c(\alpha)}{\sqrt{n}},F(x)+\frac{c(\alpha)}{\sqrt{n}}]\}$ for each KS plot. If the sampled events conform to the ground truth process at the 95% confidence level, all points in the KS plot should fall within this band.

We construct direct comparison visualizations between $F_n(x)$ and $F(x) = 1 - e^{-x}$ alongside KS plots across Transformer encoders (THP, SAHP, AttNHP) with draft length $\gamma = 10$ on three synthetic datasets. As evidenced in Fig. 4, $F_n(x)$ demonstrates strong concordance with $F(x) = 1 - e^{-x}$, and all points in the KS plots remain within the 95% confidence bands, providing robust statistical evidence for the distributional fidelity of our TPP-SD method.

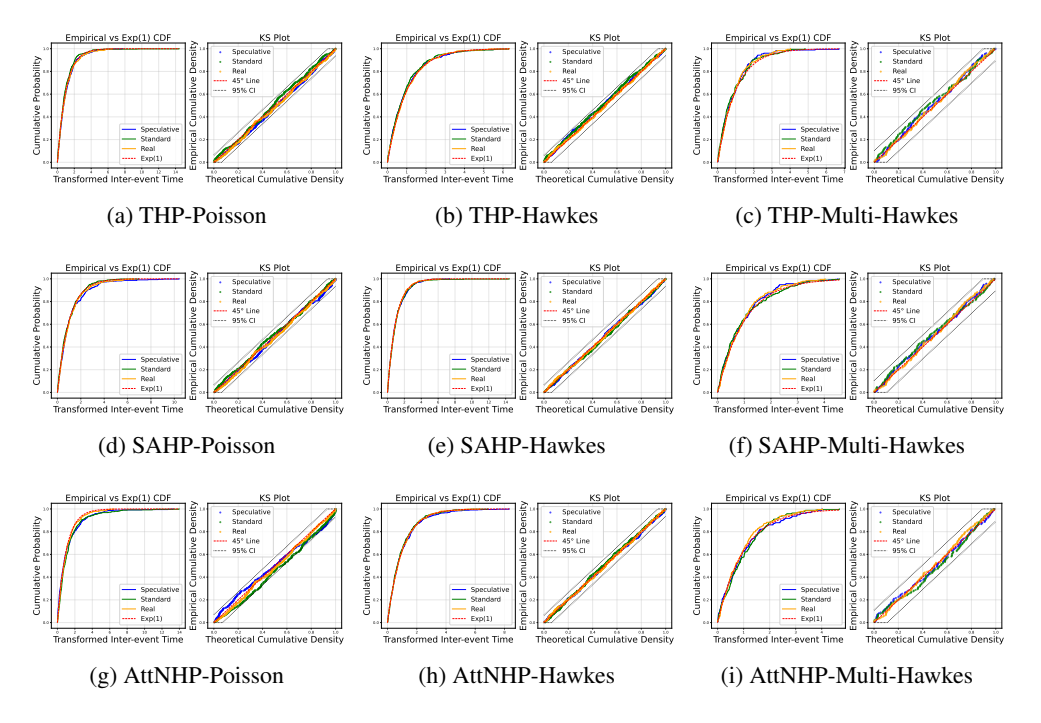


Figure 4: KS plots across THP (top row), SAHP (middle row), and AttNHP (bottom row) encoders with draft length $\gamma=10$ on three synthetic datasets: Poisson (left column), Hawkes (middle column), and Multi-Hawkes (right column). Blue, green, and orange points represent samples from TPP-SD ($\gamma=10$), AR sampling, and ground truth, respectively. Black dotted lines show 95% KS confidence bands.

C.3.2 Sampling Real-world TPPs

For the experiments in Section 5.3, we conduct evaluations within the same time window of [0,100]. In accordance with Appendix C.3.1, we report the discrepancy metric $\Delta\mathcal{L}^{\text{real}}$, the Wasserstein distance D_{WS}^t and D_{WS}^k , the execution time T_{AR} and T_{SD} for AR sampling and TPP-SD, and the resulting speedup ratio $S_{\text{AR/SD}}$ defined in Section 5.1. For computation of D_{WS}^t and D_{WS}^k , we set M=100, N=100, which means that we fix the first M=100 events as history and perform N=100 independent repetitions of sampling the 101-th event, obtaining $\{(t_i^{\text{AR}}, k_i^{\text{AR}}\}_{i=1}^{100}$ from AR sampling and $\{(t_i^{\text{SD}}, k_i^{\text{SD}}\}_{i=1}^{100}$ from TPP-SD, and subsequently computing D_{WS}^t and D_{WS}^k as elaborated in Section 5.1.

Beyond numerical metrics, we visualize event type distributions to qualitatively assess the sampling fidelity of TPP-SD on real datasets, where accurate event type sampling is critical. Figure 5 demonstrates that event type distributions from TPP-SD ($\{k_i^{\rm SD}\}$) consistently align with those from AR sampling ($\{k_i^{\rm AR}\}$) across all datasets and encoder architectures, confirming TPP-SD's ability to maintain distributional consistency with AR sampling in event type generation.

C.4 Ablation Studies

We have investigated the impact of draft length γ and draft model size on the sampling quality and sampling speed of TPP-SD with AttNHP encoder. Using the same sampling configuration and evaluation metrics as in Section 5.4, we also conducted experiments using THP and SAHP encoders.

Draft Length. As illustrated in Figs. 6a and 6b, experiments with THP and SAHP encoders reveal patterns consistent with our findings in Section 5.4: changes in draft length γ minimally affect likelihood discrepancy $\Delta \mathcal{L}$ and distance metrics D, while acceptance rate α also diminishes with increasing γ , and speedup ratio $S_{\text{AR/SD}}$ exhibits a characteristic peak followed by a decline, eventually dropping below $1\times$ when draft lengths become excessive. Intermediate draft lengths ($\gamma \approx 5$ –15) optimize computational efficiency across all experimental configurations.

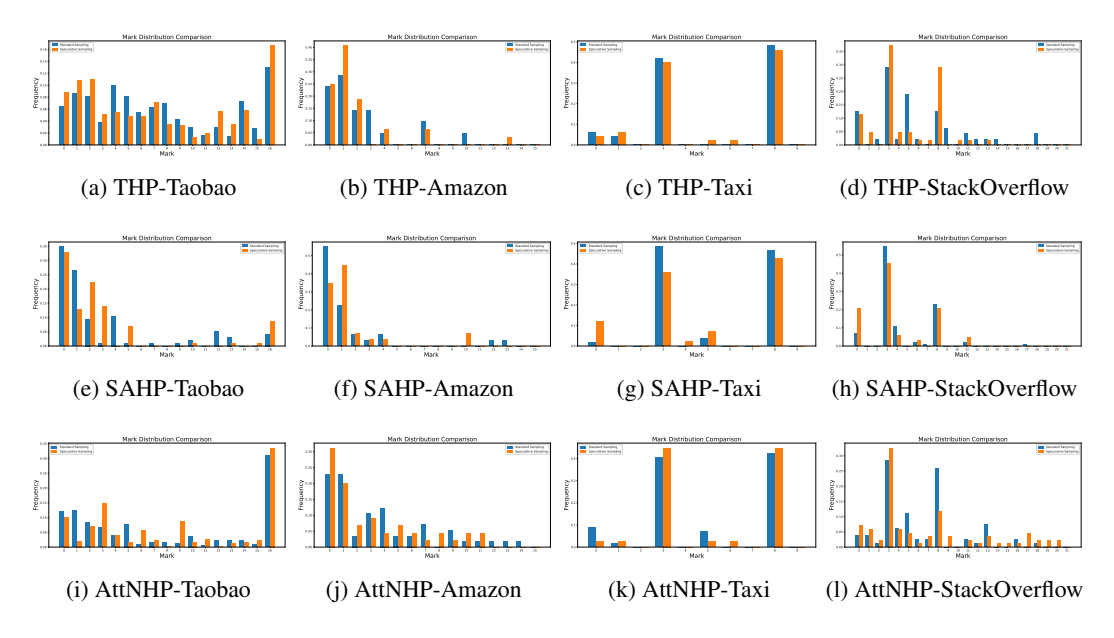


Figure 5: Event type histogram across THP (top row), SAHP (middle row), and AttNHP (bottom row) encoders with draft length $\gamma=10$ on four real datasets: Taobao, Amazon, Taxi and StackOverflow. Blue bars and orange bars represent the frequency of sampled event types from AR sampling and TPP-SD.

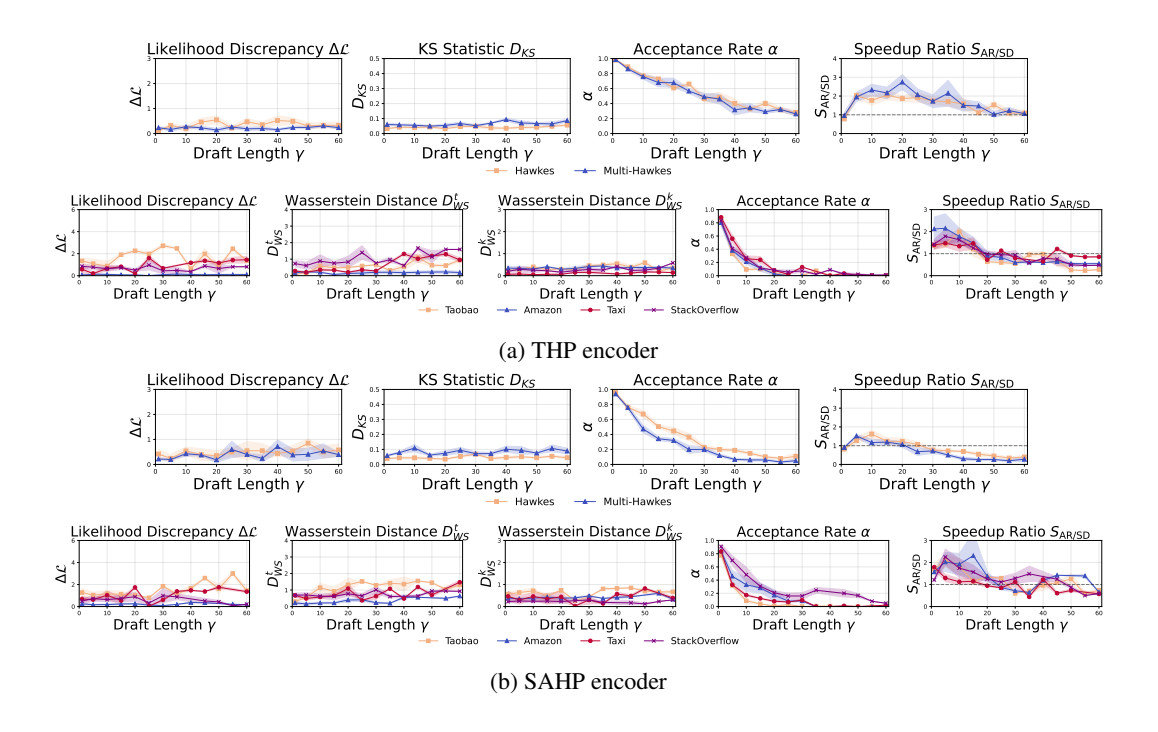


Figure 6: The impact of draft length on sampling quality measured by likelihood discrepancy ($\Delta \mathcal{L}$) and distance ($D_{\rm KS}$ or $D_{\rm WS}$), and on sampling speed measured up speedup ratio $S_{\rm AR/SD}$. We conduct experiments across five random seeds with (a) THP encoder and (b) SAHP encoder, and report the average for each metric.

Draft Model Size. As evidenced by Table 4, increasing the draft model size with either THP or SAHP encoder preserves sampling quality (measured by $\Delta \mathcal{L}$ and D) and improves the acceptance rate α , but reduces the speedup ratio $S_{\text{AR/SD}}$. The 1-head, 1-layer configuration remains optimal for the draft model across these encoder architectures.

Table 4: Performance of TPP-SD with draft length $\gamma=10$ under different size of draft model. We use KS statistic $(D_{\rm KS})$ for synthetic datasets and Wasserstein Distance $(D_{\rm WS}^t, D_{\rm WS}^k)$ for real datasets. We conducted experiments across three random seeds and report the mean for each metric. For all metrics, the best result is shown in **bold**, and the second best result is shown in <u>underline</u>.

Dataset	Encoder Type	Draft head	Model layer	$\Delta \mathcal{L}$	$D_{KS}(\downarrow)$	Distance $D_{\text{WS}}^t(\downarrow)$	$D_{\mathrm{WS}}^{k}\left(\downarrow\right)$	α (†)	Wall $T_{AR}(\downarrow)$	-time $T_{\text{SD}}(\downarrow)$	Speedup Ratio $S_{AR/SD} (\uparrow)$
Multi-Hawkes	ТНР	1 2 4	1 4 6	0.226 0.202 0.144	0.008 0.019 0.006	- - -	- - -	0.790 0.830 0.950	3.990 3.990 3.990	1.970 2.179 2.208	2.025 1.831 1.807
Multi-Hawkes	SAHP	1 2 4	1 4 6	0.054 0.143 0.395	0.008 0.004 0.008	- - -	- - -	0.640 0.740 0.800	3.543 3.543 3.543	2.143 2.669 2.734	1.653 1.327 1.296
Taobao	ТНР	1 2 4	1 4 6	0.033 0.307 0.409	- - -	0.175 0.175 <u>0.291</u>	0.222 0.339 <u>0.301</u>	0.18 0.210 0.240	5.890 5.890 5.890	3.460 3.900 4.920	1.702 1.510 1.197
Taobao	SAHP	1 2 4	1 4 6	$\begin{array}{ c c }\hline 0.410\\ \textbf{0.334}\\ 0.486\\ \end{array}$	- - -	0.302 0.403 0.545	0.630 0.742 0.745	0.14 0.19 0.21	2.460 2.460 2.460	1.621 1.850 1.990	1.518 1.330 1.236

D Additional Discussions

D.1 Why Not Use CIF-based Speculative Decoding?

In theory, CIF-based speculative decoding is feasible. For example, we can use a homogeneous Poisson process with constant intensity $\bar{\lambda}$ as the draft model to generate candidate timestamps $\{\tilde{t}_i\}$. These candidates are then input into a CIF-based Transformer point process to compute the CIF at each position, $\{\lambda^*(\tilde{t}_i)\}$, and the acceptance ratio $\{\lambda^*(\tilde{t}_i)/\bar{\lambda}\}$. A candidate timestamp t_i is accepted if all previous timestamps are accepted and $\epsilon < \frac{\lambda^*(\tilde{t}_i)}{\bar{\lambda}}$, where $\epsilon \sim \text{Uniform}[0,1]$. However, it has two significant drawbacks: (1) Determining $\bar{\lambda}$ is challenging because we must ensure that $\bar{\lambda}$ is greater than the CIF at all candidate timestamps, and the CIF values are history-dependent and stochastic. To be safe, we generally have to use a relatively large $\bar{\lambda}$, which reduces the acceptance rate and leads to low sampling efficiency. (2) The CIF-based TPP-SD may fail to generate any valid timestamp in each iteration. If the first proposed timestamp is rejected, the CDF-based TPP-SD can sample a replacement from $g_T(\tau|\cdot)$, but the CIF-based method cannot do this. This can result in cases where a single forward pass of the target model fails to generate any valid timestamp, further reducing sampling efficiency.

D.2 Necessity of Sampling from Large Target Models

A critical consideration in TPP sampling is the necessity of sampling from large draft models. For TPP data, large Transformer encoders (e.g., multi-layer, multi-head, with high-dimensional representations) are crucial for capturing complex temporal dependencies. Their larger parameter capacity allows them to model intricate data distributions and generate high-quality samples—albeit at the cost of slower autoregressive sampling. In contrast, smaller Transformer encoders (e.g., single-layer, single-head, with low-dimensional representations) are much faster at sampling due to reduced parameter capacity. However, they often struggle to model complex temporal patterns accurately, resulting in lower-quality samples that may not align well with the underlying data distribution.

To empirically demonstrate this performance gap, we evaluate a simple draft model \mathcal{M}_D (single-layer, single-head THP) on both synthetic (Poisson, Hawkes, Multi-Hawkes) and real datasets (Taxi, StackOverflow, Amazon, Taobao), measuring sampling fidelity via $\Delta\mathcal{L}$ and D_{KS} , D_{WS} , and efficiency via wall-time.

As shown in Table 5, the simplistic architecture of \mathcal{M}_D struggles to capture temporal dependencies effectively even on synthetic datasets. Performance degrades further on real datasets, with significantly

Table 5: Evaluation of sampling methods across synthetic and real-world datasets. Autoregressive sampling with the draft model (AR (draft)) consistently yields lower sample fidelity (higher $\Delta \mathcal{L}$, D_{KS} , and D_{WS}) compared to the target model (AR (target)) and our proposed TPP-SD. For each metric, the **best** result is bolded, and the second-best is underlined.

Metric	Sampling Type	Poisson	Hawkes	Multi-Hawkes	Taxi	StackOverflow	Amazon	Taobao
$\Delta \mathcal{L}(\downarrow)$	AR (draft) AR (target)	2.174 0.542	1.348 0.753	1.305 0.022	1.504 0.441	1.136 0.587	0.614 0.056	2.122 0.446
Δ ε (ψ)	TPP-SD	0.349	0.276	0.321	0.065	0.231	0.129	0.033
	AR (draft)	0.153	0.141	0.126	-	-	-	-
$D_{KS}(\downarrow)$	AR (target)	0.038	0.044	0.069	-	-	-	-
	TPP-SD	0.036	0.043	0.053	-	-	-	-
	AR (draft)	-	-	-	0.765	0.994	0.534	0.577
$D_{WS}^t(\downarrow)$	AR (target)	-	-	-	0.201	<u>0.470</u>	0.189	0.236
	TPP-SD	-	-	=	0.082	0.391	0.078	0.076
	AR (draft)	-	-	-	0.768	0.821	0.759	1.384
$D_{WS}^k(\downarrow)$	AR (target)	-	-	-	0.055	<u>0.376</u>	0.184	0.267
	TPP-SD	-	-	=	0.655	0.375	<u>0.418</u>	0.751
	AR (draft)	0.987	1.240	1.530	0.150	0.120	0.070	0.410
Wall-time (\downarrow)	AR (target)	3.477	5.147	4.007	1.157	1.353	1.023	5.890
	TPP-SD	1.647	<u>2.547</u>	<u>1.893</u>	0.453	0.700	0.290	3.460

larger $\Delta \mathcal{L}$ and D_{WS} values, as \mathcal{M}_D cannot model the complex dependencies present in the data. Draft model alone performs poorly on this task, demonstrating the necessity of a large target model and the importance of our proposed TPP-SD framework, which leverages the speed of the draft model without sacrificing the fidelity provided by the target model.

D.3 Feasibility of Using Simple Poisson Draft

The standard thinning algorithm generates candidate events using a homogeneous Poisson process $PoiP(\overline{\lambda})$. This motivates a compelling question for our TPP-SD framework: is it possible to employ a draft model as simple as $PoiP(\overline{\lambda})$ to further accelerate sampling from complex target models without compromising fidelity?

We replace the 1-head-1-layer (abbreviated as 1-H-1-L) draft model to a simple homogeneous Poisson process draft model, whose parameter is estimated by maximum likelihood estimation on the data, i.e., $\hat{\lambda} = \frac{n}{T}$, where n is the number of events and T is the time span of the dataset. As for the experiment setup, we adopt THP as the backbone of target model for illustration simplicity. We conduct the additional experiments on 3 synthetic datasets (i.e., Poisson, Hawkes, and Multi-Hawkes) and 2 real-world datasets (i.e., Taobao and Amazon).

Since Poisson process is history-independent, we can sample the candidate inter-event times τ_i all at once from $\operatorname{Exp}(\hat{\lambda})$. It is worth noting that for TPPs with marks (e.g. Multi-Hawkes), to ensure an efficient drafting process, we first estimate the mark distribution from the training data using MLE (i.e., $\hat{p}_m = \frac{n_m}{n}$, where n_m is the number of events with mark m and n is the total number of events), and then sample the marks from the estimated mark distribution all at once as well.

We can see from Table 6 that, on synthetic datasets, TPP-SD with Poisson draft maintains high fidelity in sampling while achieving even more significant speedup across three datasets. The fast drafting process of Poisson compensates for the relatively lower acceptance rate. However, on real-world datasets, while TPP-SD with Poisson draft retains the sampling fidelity, we witness drop in speedup ratio. On complex real-world TPPs, the acceptance rate of Poisson draft is too low that it overwhelms the speedup from fast drafting. Therefore, in our setting of TPP-SD, we use a more robust drafting strategy, i.e., a slightly more complex draft model (1-layer-1-head THP) to ensure that TPP-SD can achieve high fidelity sampling across a wide range of datasets.

D.4 Architectural Differences across Encoders

We incorporate the history encoders from THP, SAHP, and AttNHP into our CDF-based Transformer TPPs designed for TPP-SD. The architectural and implementation differences among these encoders may explain the varying sampling speed performance observed in Table 1 and Table 2.

Table 6: Comparison between a 1-head-1-layer (1-H-1-L) Transformer draft model and a simple Poisson process draft within the TPP-SD framework. On synthetic data, the Poisson draft achieves a higher speedup at the cost of fidelity. On real-world data, its low acceptance rate leads to inferior performance in both speed and fidelity. For each metric, the **best** result between the two TPP-SD methods is bolded, and the second-best is underlined.

Dataset	Sampling Method	$\Delta \mathcal{L}(\downarrow)$	$D_{KS}(\downarrow)$	$D^t_{WS}(\downarrow)$	$D^k_{WS}(\downarrow)$		$\begin{array}{c} \textbf{Speedup} \\ S_{AR/SD}(\uparrow) \end{array}$
	AR Sampling	0.542	0.038	-	-	-	-
Poisson	TPP-SD (1-H-1-L draft)	0.349	0.036	-	-	0.740	2.110
	TPP-SD (Poisson draft)	0.630	0.050	-	-	<u>0.370</u>	3.230
	AR Sampling	0.753	0.044	-	-	-	-
Hawkes	TPP-SD (1-H-1-L draft)	0.276	0.043	-	-	0.720	2.113
	TPP-SD (Poisson draft)	0.286	0.036	-	-	<u>0.520</u>	5.430
	AR Sampling	0.022	0.069	-	-	-	-
Multi-Hawkes	TPP-SD (1-H-1-L draft)	0.321	0.053	-	-	0.750	2.117
	TPP-SD (Poisson draft)	0.268	0.057	-	-	0.390	3.610
	AR Sampling	0.446	-	0.236	0.267	-	-
Taobao	TPP-SD (1-H-1-L draft)	0.033	-	0.076	0.751	0.260	1.597
	TPP-SD (Poisson draft)	0.680	-	0.091	0.623	<u>0.030</u>	<u>1.370</u>
	AR Sampling	0.056	-	0.189	0.184	-	-
Amazon	TPP-SD (1-H-1-L draft)	0.129	-	0.078	0.418	0.270	3.550
	TPP-SD (Poisson draft)	0.066	-	0.090	0.086	<u>0.010</u>	<u>2.230</u>

Following the notation in Section 4.2, the temporal encoding $\mathbf{z}(t_i) \in \mathbb{R}^D$ for each encoder differs slightly:

THP:
$$[\mathbf{z}(t_i)]_j = \begin{cases} \sin(t_i/10000^{j/D}) & j \text{ is even} \\ \cos(t_i/10000^{(j-1)/D}) & j \text{ is odd} \end{cases}$$
, (27)

SAHP:
$$[\mathbf{z}(t_i)]_j = \begin{cases} \sin(j/10000^{j/D} + w_j t_i) & j \text{ is even} \\ \cos(j/10000^{(j-1)/D} + w_j t_i) & j \text{ is odd} \end{cases}$$
, (28)

AttNHP:
$$[\mathbf{z}(t_i)]_j = \begin{cases} \sin(t_i/m \cdot (5M/m)^{j/D}) & j \text{ is even} \\ \sin(t_i/m \cdot (5M/m)^{(j-1)/D}) & j \text{ is odd} \end{cases}$$
 (29)

where $[\mathbf{z}(t_i)]_j$ is the j-th dimension of the temporal embedding vector $\mathbf{z}(t_i)$, and M, m are hyperparameters in AttNHP.

The attention mechanisms differ across encoder architectures. For clarity, we present the single-head attention formulation for each model. The layer-l history embedding of event (t_i, k_i) is computed as:

THP/SAHP:
$$\mathbf{h}^{(l)}(t_i) = \mathbf{h}^{(l-1)}(t_i) + \sum_{j=1}^{i} \frac{f(\mathbf{q}^{(l)}(t_j), \mathbf{k}^{(l)}(t_i))\mathbf{v}^{(l)}(t_j)}{\sum_{j=1}^{i} f(\mathbf{q}^{(l)}(t_j), \mathbf{k}^{(l)}(t_i))},$$
 (30)

AttNHP:
$$\mathbf{h}^{(l)}(t_i) = \mathbf{h}^{(l-1)}(t_i) + \tanh\left(\sum_{j=1}^{i} \frac{f(\mathbf{q}^{(l)}(t_j), \mathbf{k}^{(l)}(t_i))\mathbf{v}^{(l)}(t_j)}{1 + \sum_{j=1}^{i} f(\mathbf{q}^{(l)}(t_j), \mathbf{k}^{(l)}(t_i))}\right),$$
 (31)

where $f(\cdot,\cdot)$ is a Gaussian kernel $f(\mathbf{q}^{(l)}(t_j),\mathbf{k}^{(l)}(t_i)) = \exp(\frac{1}{\sqrt{D}}\mathbf{q}^{(l)}(t_i)^{\top}\mathbf{k}^{(l)}(t_j)) \in \mathbb{R}$. The key distinction lies in how query, key, and value vectors are derived at layer-l. In THP and SAHP, $\mathbf{q}^{(l)}(t_i) = \mathbf{Q}^{(l)}\mathbf{h}^{(l-1)},\mathbf{k}^{(l)}(t_i) = \mathbf{K}^{(l)}\mathbf{h}^{(l-1)},\mathbf{v}^{(l)}(t_i) = \mathbf{V}^{(l)}\mathbf{h}^{(l-1)}$ are obtained through linear projection, whereas in AttNHP:

$$\mathbf{q}^{(l-1)}(t_i) = \mathbf{Q}^{(l)} \operatorname{concat}(1; \mathbf{z}(t_i)^\top; \mathbf{h}^{(l-1)}(t_i)^\top)^\top, \tag{32}$$

$$\mathbf{k}^{(l-1)}(t_i) = \mathbf{K}^{(l)} \operatorname{concat}(1; \mathbf{z}(t_i)^\top; \mathbf{h}^{(l-1)}(t_i)^\top)^\top, \tag{33}$$

$$\mathbf{v}^{(l-1)}(t_i) = \mathbf{V}^{(l)} \operatorname{concat}(1; \mathbf{z}(t_i)^\top; \mathbf{h}^{(l-1)}(t_i)^\top)^\top, \tag{34}$$

where $\mathbf{Q}^{(l)}, \mathbf{K}^{(l)}, \mathbf{V}^{(l)} \in \mathbb{R}^{D \times (2D+1)}$. AttNHP's complex attention mechanism doubles the dimension of intermediate vectors, particularly in multi-head configurations where each head requires

separate query, key, and value transformations. This architectural complexity results in significantly higher AR sampling latency compared to other models, making AttNHP an ideal candidate for acceleration via TPP-SD, where it achieves the largest speedup. Despite architectural similarities between THP and SAHP, implementation differences result in SAHP consistently achieving the shortest wall-time for both AR sampling and TPP-SD, leaving less room for additional acceleration.

D.5 Differences between TPP Sampling and Long-horizon Prediction

While both TPP sampling and long-horizon prediction [35, 24] involve generating sequences of events over a continuous time interval given some history, they have fundamental differences. TPP sampling focuses on generating events from the correct distribution. Since sampling is inherently stochastic, comparing the exact events sampled with specific test set events isn't meaningful - the same distribution that we sample from can produce different event in each iteration. What matters is whether the sampled sequences follow the correct statistical patterns. On synthetic datasets, we evaluate the distributional conformity of sampled sequences from TPP-SD to the ground truth using [2] and KS statistic. On real datasets, we measure the distributional discrepancy between the sampled sequences from autoregressive sampling and TPP-SD with Wasserstein distance.

In contrast, long-horizon prediction specifically aims to forecast future events that closely match the ground truth on the test set. It's evaluated by metrics such as RMSE and optimal transport distance (OTD) that directly measure the discrepancy between predicted sequences and test-set sequences.

D.6 Limitations

Compared to the thinning algorithm, our proposed TPP-SD is deep-learning based which requires large amount of event sequence data to learn the model's parameters. Therefore, the model is less suitable for sampling in data-scarce scenarios.

Besides, TPP-SD adopts the original SD framework from the LLM domain and requires deploying two models at the same time for accelerating sampling, which is slightly more computational demanding and less convenient. Recent advances in SD techniques [3, 16] can be incorporated to further optimize TPP-SD, and we leave this as future work.